Error characterization of methane fluxes and budgets derived from a long-term comparison of open- and closed-path eddy covariance systems

M. Julian Deventer[a,*], Timothy J. Griffis[a], D. Tyler Roman[b], Randall K. Kolka[b], Jeffrey D. Wood[c], Matt Erickson[a], John M. Baker[a,d], Dylan B. Millet[a]

[a] University of Minnesota – Dept. Soil, Water & Climate, United States
[b] US Forest Service – Northern Research Station Grand Rapids, United States
[c] University of Missouri – School of Natural Resources, United States
[d] US Department of Agriculture – Agricultural Research Service, United States

ABSTRACT

Wetlands represent the dominant natural source of methane (CH_4) to the atmosphere. Thus, substantial effort has been spent examining the CH_4 budgets of global wetlands *via* continuous ecosystem-scale measurements using the eddy covariance (EC) technique. Robust error characterization for such measurements, however, remains a major challenge. Here, we quantify systematic, random and gap-filling errors and the resulting uncertainty in CH_4 fluxes using a 3.5 year time series of simultaneous open- and closed path CH_4 flux measurements over a sub-boreal wetland.

After correcting for high- and low frequency flux attenuation, the magnitude of systematic frequency response errors were negligible relative to other uncertainties. Based on three different random flux error estimations, we found that errors of the CH_4 flux measurement systems were smaller in magnitude than errors associated with the turbulent transport and flux footprint heterogeneity. Errors on individual half-hourly CH_4 fluxes were typically 6%–41%, but not normally distributed (leptokurtic), and thus need to be appropriately characterized when fluxes are compared to chamber-derived or modeled CH_4 fluxes.

Integrated annual fluxes were only moderately sensitive to gap-filling, based on an evaluation of 4 different methods. Calculated budgets agreed on average to within 7% ($\leq 1.5\,g - CH_4\,m^{-2}\,yr^{-1}$). Marginal distribution sampling using open source code was among the best-performing of all the evaluated gap-filling approaches and it is therefore recommended given its transparency and reproducibility.

Overall, estimates of annual CH_4 emissions for both EC systems were in excellent agreement (within $0.6\,g - CH_4\,m^{-2}\,yr^{-1}$) and averaged $18\,g - CH_4\,m^{-2}\,yr^{-1}$. Total uncertainties on the annual fluxes were larger than the uncertainty of the flux measurement systems and estimated between 7–17%. Identifying trends and differences among sites or site years requires that the observed variability exceeds these uncertainties.

1. Introduction

The recent debate regarding the causes of an apparent plateau in atmospheric methane (CH_4) concentrations during the early 2000 s reflects gaps in our current understanding of its climate-sensitive sources and sinks and their variability (Kirschke et al. 2013; Schaefer et al. 2016; Saunois et al., 2016; Poulter et al., 2017). This uncertainty impairs confidence in climate projections due to methane's large global warming potential (GWP), 28–36 times larger than that of carbon dioxide (CO_2) on a 100 year time horizon (Myhre et al. 2013). Global CH_4 inventories exhibit large variability between bottom-up approaches versus top-down estimates (Kirschke et al. 2013; Saunois et al., 2016),

but generally agree that the integrated biogenic CH_4 source is comparable in size to the anthropogenic flux. Microbial CH_4 production in anaerobic wetland soils is the largest biogenic source, and is believed to result in more CH_4 emissions than the global production and use of fossil fuels (Kirschke et al. 2013; Saunois et al., 2016).

While wetlands cover a relatively small fraction of Earth's land surface ($\sim 10\%$, Rebelo et al., 2009) their contribution to the global surface-atmosphere flux of CH_4 and thus to the Earth's radiative forcing is disproportionally large. Representative measurements are thus needed to assess how CH_4 emissions from wetlands respond to hydro-meteorological and land management factors, and to build a process understanding for projecting future changes. Eddy covariance (EC)

---

* Corresponding author.
  E-mail address: deventer@umn.edu (M.J. Deventer).

(Baldocchi et al. 1988) is currently the most widely used methodology for measuring surface-atmosphere exchange of greenhouse gases (GHG) at the ecosystem scale. While networks have been initiated around the world to create a standardized global flux monitoring program and database (FLUXNET) (Baldocchi et al. 2001), CH_4 is not yet a fully integrated product in the resulting synthesized datasets available to the public. We therefore lack a measurement-based benchmark for top-down inversion-based CH_4 budgets. Two international efforts have recently been initiated to better constrain CH_4 observations: (i) The Global Carbon Project (http://www.globalcarbonproject.org/) launched a CH_4 flux synthesis effort with the aim of collating flux data from the global ensemble of terrestrial observations, identifying data limitations and inconsistencies, and deriving standardization guidelines for future inclusion into FLUXNET and gridded CH_4 products (AmeriFlux, 2018); and (ii) the pan-European Research Infrastructure Integrated Carbon Observatory System (ICOS) published the first protocol for standardization of high frequency CH_4 measurements, flux calculation and quality control (Nemitz et al., 2018). Both of these projects follow the tradition of the micrometeorological community in unifying and (openly) releasing flux calculation algorithms within collaborative network activities (e.g. Fratini and Mauder 2014; Mammarella et al., 2016).

The foundation of any EC flux measurement system is a fast analyzer capable of resolving turbulent fluctuations of the target species at appropriate precision (Baldocchi et al. 1988). Laser absorption spectroscopy-based methane gas analyzers have been tested for their applicability in EC flux measurements in the past (Tuzson et al. 2010; Detto et al. 2011; Peltola et al. 2013, 2014; Iwata et al. 2014); however, intercomparison studies have only been carried out over relatively short duration (a few weeks to months), with the exception of a single year-long study conducted in the arctic (Goodrich et al. 2016). In terms of absolute fluxes, the above studies reported good agreement between different CH_4 analyzer technologies, but also highlighted that sensor-specific corrections (e.g. for density fluctuations and water vapor interference) can be of the same magnitude or larger than the measured fluxes. Further, open-path EC systems were reported to have poor data coverage during freezing or rainy periods and in locations with ubiquitous high humidity or sea spray. Thus, a large fraction of the measured time series often needs to be gap-filled for budget calculations. As a result, there is a need to better understand the effects of such corrections and gap-filling uncertainties on annual CH_4 flux budgets, which may in turn be broadly used in the climate science community.

Here, we present CH_4 flux measurements from a natural wetland site over the course of 3.5 years (January 2015–July 2018) using two commercially available CH_4 gas analyzers. These systems include an open-path CH_4 gas analyzer (LI-7700, LI−COR Biosciences Inc., Lincoln, NE, USA) and a closed-path tunable diode laser (TGA-100A, Campbell Scientific, Logan, UT, USA). Both CH_4 flux systems rely on shared turbulence measurements and thus have identical flux footprints. This unique dual-sensor dataset features a large number of paired observations across a wide spectrum of hydro-meteorological variability enabling a statistically robust analysis of the measured fluxes, their precision, detection limits and consistency. Taking advantage of these concurrent measurements we evaluate the most commonly used methods for flux error estimation against the directly observed distribution of flux differences, which we here interpret as the uncertainty of the flux measurement system. We further quantify the uncertainty introduced across differing correction methods for systematic errors arising from imperfect sampling of turbulent fluctuations. Next, we characterize the errors associated with gap-filling flux time series to derive yearly CH_4 budgets and quantify the resulting annual uncertainties. Finally, we give recommendations for processing and characterizing annual CH_4 flux products, and demonstrate the importance of accurate uncertainty estimation for interpreting measured wetland fluxes.

2. Methods

2.1. Site description

Eddy covariance measurements were carried out at the Bog Lake Fen flux tower site in the USDA Forest Service's Marcell Experimental Forest (47.505 N, −93.489 W, Minnesota, USA). The flux tower is located in an open natural peatland, characterized as poorly minerotophic to oligotrophic (mean pore water pH = 4.5, range 3.8–5.3) with the dominant vegetation consisting of *Sphagnum papilosum*, *Scheuzeria palustris, Carex spp*., and *Chamaedaphne calyculata* (Shurpali et al. 1993, 1995). Bog Lake Fen soils are mapped as the Greenwood series (Dysic, frigid Typic Haplohemists), with peat depth of about 2 m at the EC tower. The bog has complex micro-topography, with a mosaic-like hummock-hollow surface pattern and water balance driven largely by precipitation (roughly half of precipitation falls as snow) and evaporation, since no surface water outlet is present. The climate is cold continental with warm summers (Köppen Dfb, Kottek et al. (2006)), with mean annual precipitation and temperature of 770 mm and 3 °C, respectively. The snow-covered period usually starts in November and typically lasts for ~120 days.

2.2. Instrumentation

Three-dimensional wind velocity and sonic temperature measurements were made using an ultrasonic anemometer (CSAT-3, Campbell Scientific) mounted 2.4 m above the surface. An open path CO_2 and H_2O infrared gas analyzer (LI-7500A, LI−COR Biosciences Inc.) was positioned at the same height (in reference to the center of its measurement path) and offset by 10 cm to the east. High frequency CH_4 concentrations were measured with two instruments: a low-power open path analyzer (LI-7700, LI−COR Biosciences Inc.), and a closed path trace-gas analyzer (TGA100A, Campbell Scientific), both employing laser spectroscopy. Whereas several closed-path instruments for fast and high precision CH_4 measurements are commercially available, the LI-7700 is the first instrument of its kind that can be operated with very limited power and infrastructure, as neither temperature control nor pumps are required. Typical noise levels for both instruments are 5–10 nmol mol^{-1} (Allan deviation at 10 Hz). Details and configuration of the two CH_4 gas analyzers are provided in Table 1. Data from all eddy flux sensors were recorded at 10 Hz frequency. Gas-analyzers were calibrated twice per year (step calibration), to reflect changes between cold and warm seasons. Ancillary measurements at the tower site included basic meteorology, soil temperature, soil heat flux and water table position (Table 1) More details about the flux tower site can be found in Shurpali et al. (1993; 1995), and Olson et al. (2013).

2.3. Eddy covariance methodology

Vertical turbulent fluxes were calculated using the eddy covariance method according to the general equation (Webb et al. 1980):

$$F = \overline{(w \rho)' c'} \tag{1}$$

Where, w is the vertical wind speed, ρ is air density, c is an atmospheric scalar, primes denote turbulent fluctuations, and overbars denote means obtained from time averaging over the flux interval, here set to 30 min. The scalar and sonic anemometer time series were aligned using supervised cross correlation maximization after a double-axis rotation was performed on measured wind vectors. De-spiking of high frequency data (Vickers & Mahrt, 1997) was not performed because a test analysis using a subset of the data revealed that the number of identified spikes and their effect on the post-processed fluxes were negligible (< 1%).

The sensible heat (H), latent heat (LE) and CO_2 (NEE) fluxes were calculated following standard procedures as documented elsewhere

Table 1

Methane gas analyzer configurations and auxiliary measurements.

	CH$_4$ sensor	
	TGA-100A	LI-7700
type	closed path	open path
laser	led-salt diode laser	tunable diode laser in open Herriott cell
cell	153.08 cm path length	open Herriott cell, 47 cm path length
	480 ml volume	
effective time constant	< 0.04 s	< 0.025* s
cell residence time	< 0.1 s	n.a.*
configuration	liquid N$_2$ cooled, Nafion Drier PD200T	
power (typical)	> 300 W	8 W
height	2.4 m (inlet)	2.4 m (ref.: center of measurement path)
tube length	3.4 m	n.a.
tube diameter	4.3 mm	n.a.
flow rate	15 slpm	n.a.
pump	Bush Model RB0021	n.a.
separation	4 cm	49 cm

	auxiliary measurements		
variable	location	model	manufacturer
soil temperature	5,10,20,30,40,50,100,200 [cm depth]	T107	Campbell Scientific
air temperature	2 [m height]	HMP45C	Campbell Scientific
relative humidity	2 [m height]	HMP45C	Campbell Scientific
precipitation	1.5 [m height]	TE-525 tipping bucket rain gauge	Texas Electronics
wind speed	3 [m height]	05103 wind monitor	R. M. Young
wind direcon	3 [m height]	05103 wind monitor	R. M. Young
PAR	3 [m height]	LI190-SB quantum sensor	LI-COR Biosciences
radiation	2 [m height]	CNR4 Net Radiometer	Kipp and Zonen
soil heat flux	10,10,10 [cm depth]	HFP01-SC heat flux plate	Hukseflux
water table position	1.5 [m distance to EC tower]	FW-1 stripchart recorder	Belfort

(e.g. Foken et al., 2012). Methane fluxes based on TGA mixing ratio (χ_{CH4}) measurements were calculated according to:

$$F_{CH_4} = \overline{\rho_a} \cdot \overline{w' \chi'_{CH_4}} \tag{2}$$

Density fluctuations were assumed to be removed by drying and heating of the sample air prior to analysis. Fluxes based on mass density (ρ_{CH_4}) measurements by the LI-7700 were calculated according to McDermitt et al. (2011):

$$F_{CH_4} = A(\overline{w'\rho'_{CH_4}} + B\mu\frac{\overline{\rho_{CH_4}}}{\overline{\rho_a}}\overline{w'\rho'_{H_2O}} + C\frac{(1+\mu\sigma)\overline{\rho_{CH_4}}}{\overline{T}}\overline{w'T'}) \tag{3}$$

Where, A, B, and C are dimensionless multipliers to correct for spectroscopic effects caused by temperature- and pressure –induced line-broadening, μ is the molar mass ratio of dry air to water vapor, $\overline{\rho_a}$ is the average mass density of dry air, σ is the mass density ratio of water vapor to dry air, ρ_{H_2O} is the water vapor mass density, and T is air temperature. The second and third terms in the parentheses are the traditional Webb, Pearman, Leuning (WPL) terms (Webb et al., 1980). The contribution of WPL and spectroscopic terms to calculated fluxes are discussed in detail in Text S1 and Fig. S1, 2. Storage flux terms were quantified using a simple 1-level approach (Rannik et al., 2009), but were found to be negligible. Furthermore, since storage affects NEE measured by both CH$_4$ systems equally, no effect on flux comparisons is expected, and therefore no corresponding adjustment was performed.

2.3.1. Post-processing of time series data

The closed path TGA system was designed to operate at stable temperatures and pressures, and during our campaign the laser temperature and cell pressure were both maintained to a high degree of precision. However, the TGA cell temperature was also affected by the instrument's enclosure temperature, which is intended to be maintained at a stable set-point above ambient. At Bog Lake Fen, ambient temperatures were highly variable, especially during the cold season when diurnal amplitudes exceeded 20 °C and 24-h maxima varied by up to 16 °C between consecutive days. As a result, the control software was at times unable to maintain stable enclosure (and hence cell)

temperatures, resulting in low-frequency drifts in the CH$_4$ signal for ~10% of observations, as indicated by the instrument's diagnostic value for heater cycling. Such drift was not apparent in the concurrent LI-7700 measurements, nor in other measured scalars such as CO$_2$ or sonic temperature (Fig. S3). These low frequency fluctuations manifested as a positive slope in the Allan variance at time scales exceeding several seconds (Fig. S4). We therefore interpret this behavior as a TGA-specific optical fringing effect due to temperature drifts; similar artifacts in TGA measurements have been observed at other sites (Mammarella et al., 2016; Jackowicz-Korczyński et al., 2010). To account for the occasionally observed optical fringing effects and to keep post-processing routines consistent, the CH$_4$ time series for both analyzers were de-trended by subtracting the corresponding running mean, calculated using a first order autoregressive filter with τ = 30 s time constant (McMillen, 1988; Rannik and Vesala, 1999).

2.3.2. Spectral corrections

Fluxes were corrected for low and high-pass filtering effects introduced by de-trending and by the limited high frequency response of the respective measurement systems. Here, we used two established routines to (i) theoretically (e.g. Moore 1986) and (ii) empirically (Aubinet et al., 1999; Foken et al., 2012) estimate the resulting flux attenuation. In the theoretical case, transfer functions were obtained from the superposition of individual analytically formulated response terms for (a) dynamic/time response, (b) path (LI-7700) or volume (TGA) averaging, (c) lateral sensor separation, and in the case of the TGA system (d) low-pass filtering associated with attenuation in the intake tube. Additionally, (e) a response term from the autoregressive filter was implemented to account for high-pass filtering (Moore 1986, Rannik & Vesala 1999; Massman, 2000, 2001, Horst and Lenschow, 2009).

In the empirical approach, transfer functions were determined as the ratio of the integrated attenuated scalar cospectra to the integrated unattenuated temperature cospectra, here considered to be the idealized spectra. To reduce uncertainties, especially in the low-frequency range, data were screened for consecutive 3-hr periods fulfilling the

steady-state test (**2.3.4**) following the recommendation of Aubinet et al. (1999):

$$H(f)^{emp.} = \frac{N_\theta}{N_c} \frac{C_{wc}(f) df}{C_{w\theta}(f) df}, \; with \; \frac{N_\theta}{N_c} = \frac{\int_{f0}^{f1} C_{w\theta}(f) \, df}{\int_{f0}^{f1} C_{wc}(f) \, df} \tag{4}$$

Where, N_θ and N_c are normalization factors calculated as the ratio of integrated cospectral densities in a frequency (f) band where flux attenuation is assumed to be negligible (f_0 to f_1, here ≈ 0.02 to 0.07 Hz). C_{wx} are the cospectral densities of vertical wind and the scalar (c) or sonic temperature (θ). Cospectra were calculated following Nordbo & Katul (2013) (Text S5).

Absolute spectral flux losses δ_{F_c} were estimated as the ratio of the attenuated cospectral density to the idealized cospectral density:

$$\frac{\delta_c}{F_c} = 1 - \frac{\int_0^\infty C_{ws}(f) \cdot H(f) df}{\int_0^\infty C_{ws}(f) \, df} \tag{5}$$

Where, f is the natural frequency, C_{ws} is the idealized cospectrum, and H is an EC system-specific transfer function. The right-hand fraction in Eq. (5) is the inverse of the spectral correction factor (SCF), i.e. the factor needed to increase the attenuated covariance to match the reference covariance. Spectral corrections were applied before fluxes were calculated (e.g. by replacing $\overline{w'\rho'_{CH_4}}$ with $SCF \cdot \overline{w'\rho'_{CH_4}}$ in Eq. (3)).

2.3.3. Data quality control & retention

Fluxes were filtered by testing the high frequency data for stationarity < 1, $-2 <$ skewness < 2, < 1 kurtosis < 8, and intermittency < 1, as well as for-well-developed turbulence (ITC$_w$ < 0.6) (Foken and Wichura 1996, Vickers and Mahrt, 1997). Additionally, a nighttime friction velocity threshold was investigated using both CH$_4$ and CO$_2$ observations (Papale et al., 2006) but not implemented in this study as evidence for systematic underestimation of nocturnal CH$_4$ fluxes was ambiguous and resulting corrections were marginal (Text S4). Along with the flux periods removed by the QC procedures, data were also lost during periods of sensor malfunction and servicing. For the LI-7700, data were likewise lost when the measurement path was temporarily obstructed, as monitored by the instrument's relative signal strength indicator (RSSI) measuring the current received at the detector and by other relevant diagnostics. In our case, data were deemed unusable if more than 2% of the high frequency data within a flux averaging period showed RSSI < 40. Finally, flux data for all sensors were discarded if the wind direction measurements indicated possible flow distortion due to tower interference, or contributions to flux footprints from surrounding upland forests (from 30° to 200°). Over 3.5 years, there were n $\approx 23,000$ (TGA) and n $\approx 19,000$ (LI-7700) fluxes measured during periods with acceptable instrument diagnostics and winds from the peatland sectors. The LI-7700 instrument was not operated before March 2015, and thus lacks data for 75 days at the beginning of the campaign. After quality control, the datasets retained 62% of the measured peatland fluxes (n = 15,033) for the TGA and 76% of the measured peatland fluxes (n = 14,106) for the LI-7700. Overall, this represented 24% of half-hour periods within the 3.5-year campaign, lower retention than for the CO$_2$/H$_2$O EC system (38%). This data retention is on the low end of reported values (24% to 65%) from (multi) yearlong CH$_4$ flux measurements in wetland systems (Goodrich et al., 2016; Rinne et al., 2007; Kroon et al., 2010; Hommeltenberg et al., 2014; Jackowicz-Korczyński et al., 2010; van den Berg et al., 2016; Wang et al., 2017).

2.4. Flux uncertainties and limits of detection

The measured flux includes the true flux ($\hat{F}$) plus random ($\in$) and systematic (δ) error components for measurement system (x) at time (t):

$$F_{t,x} = \hat{F}_t + \in_{t,x} + \delta_{t,x} \tag{6}$$

Systematic error can result from (i) mis-calibration of instrumentation, (ii) incomplete sampling of turbulent fluctuations, (iii) lack of observations of non-turbulent fluxes during poorly mixed conditions and, (iv) the potential underestimation of EC derived energy fluxes that are used for calculation of the WPL terms (Richardson et al., 2012). As described in Section 2.3.2 and Text S4, we corrected for (ii) and estimated the magnitude of (iii) to be within 1% on annual fluxes. While spectral corrections induce uncertainties of their own, we nevertheless assume here that after spectral corrections, remaining $\in_{t,x} \gg \delta_{t,x}$.

The random flux error contains contributions from sources such as errors arising from the stochastic nature of turbulence due to limited sampling in time and space, errors of the flux measurement system (both in measurements and flux calculation), and uncertainty regarding the spatial representativeness (flux footprint) of the calculated flux (Richardson et al., 2012). The turbulent transport error (from here on called "sampling error") has been discussed as the largest contributor to random flux errors in forest eco systems (Hollinger & Richardson 2005). Here, we employ two single-instrument approaches for estimating sampling errors (σ_F). First σ_F was inferred in a one-point statistical estimation as the variance of the wind-scalar covariance $\sigma^2_{\overline{w'c'}}$ following (Finkelstein & Sims, 2001), hereafter referred to as F&S:

$$\sigma_F = \sqrt{\sigma^2_{\overline{w'c'}}} = \{\frac{1}{n} [\sum_{p=-m}^{m} \overline{w'w'}(p) \, \overline{c'c'}(p) + \sum_{p=-m}^{m} \overline{w'c'}(p) \, \overline{c'w'}(p)]\}^{1/2} \tag{7}$$

Where, the auto- ($\overline{x'x'}(p)$) and cross-covariance ($\overline{x'y'}(p)$) terms for vertical wind and the scalar of interest were integrated over the time-window defined by m, here set to 200 (i.e. 20 s), p is the index of samples, and n is the number of observations in each flux averaging interval. The fractional flux error was then calculated by dividing the absolute flux error by the measured covariance ($\frac{\sigma_F}{w'c'}$). The F&S approach has been evaluated as a physically meaningful estimator for turbulence driven uncertainties in eddy fluxes (Rannik et al., 2016). It does not incorporate uncertainty due to footprint heterogeneity nor the flux calculation.

In our second single-instrument approach (hereafter called the H&R approach), the flux errors were estimated from the difference in fluxes measured 24-h apart under similar meteorological conditions (soil temperatures within 0.5 °C) (Hollinger & Richardson, 2005). As with the F&S approach above, the H&R approach was performed separately for each eddy flux system. In contrast to the F&S approach, this error estimate also incorporates the uncertainty related to the footprint heterogeneity. In the past functional agreement between the H&R error and turbulent sampling error has been found, however the H&R method yielded larger error estimates reflecting the fact that the H&R approach also includes footprint heterogeneity (Hollinger & Richardson, 2005).

In addition to the two single-instrument approaches, we derived an estimate of the random flux error associated with the CH$_4$ flux measurement system itself, based on the contemporaneous CH$_4$ flux differences between the TGA and LI-7700 systems (i.e. differences in paired observations in time; hereafter referred to as the PD approach). Since both CH$_4$ flux systems were based on the same realization of turbulence (shared sonic anemometer), neither turbulent sampling errors nor uncertainty of the flux footprint affected the distribution of paired differences. Thus (after minimizing systematic spectral losses

beforehand) we hypothesize that PD derived errors were caused primarily by flux calculations, which differed fundamentally between the two CH_4 measurement systems. For instance, the LI-7700 measurements were affected by density fluctuations and estimates of the WPL terms (Eq. 3), whereas the TGA measurements were based on mixing ratios (Eq. (2)). In light of the ongoing effort for a global synthesis of CH_4 flux observations the PD derived errors are particularly relevant. Specifically, it is of interest to examine how its magnitude compares to the turbulent sampling and footprint error, which typically are accepted as a reasonable estimation of the total random flux error (Hollinger and Richardson 2005). Further, differences between paired observations can reveal the long-term cumulative effects of errors and bias (Dragoni et al., 2007), which cannot be readily predicted or modeled.

Instrument noise for both the vertical wind and scalar measurements contribute to the total random flux errors. For this study, we assumed that the former is negligible compared to the latter (Rannik et al., 2016), and compute the covariance error due to scalar sensor noise (σ_n) following (Lenschow et al., 2000):

$$\sigma_n = \sqrt{\frac{\sigma_w^2 \sigma_{c\_nf}^2}{fT}},$$

(8)

Where, σ_w^2 is the variance of the vertical wind measurements, and $\sigma_{c\_nf}^2$ is the noise (n) variance of the scalar sensor at frequency (f) for flux averaging interval (T). $\sigma_{c\_nf}^2$ was approximated as the difference between the scalar signal variance and the scalar signal auto-covariance at close to zero shift (here: lag = 5).

Flux detection limits were calculated following Wienhold et al. (1995). Specifically, the 95% confidence interval of the detection limit was estimated as 1.96 times the standard deviation of the cross-covariance function between the vertical wind and the CH_4 time series for lags larger than the integral time scale (here: $100 < |lags| < 200$ s).

2.5. Methane budget and gap filling

To calculate annual CH_4 budgets, the EC time series required a gap-filling strategy. Here we investigated the applicability and uncertainties of 3 different approaches:

2.5.1. Approach A: extrapolating 30-min fluxes to daily fluxes with subsequent gap-filling based on observed soil temperature response

Valid 30-min CH_4 fluxes were extrapolated to a daily value if there were a sufficient number of observations (here set to 8) for that day. To estimate the associated uncertainty, this threshold was iteratively increased from 8 to 16 half hours (1/6th to 1/3rd of possible observations per day). Further, we randomly introduced artificial data gaps (25% of observed 30-min fluxes each iteration) for $n = 50$ iterations to assess extrapolation errors.

After extrapolation, the daily flux time series still included data gaps with lengths $\geq$ 1 day. To fill these gaps, we parameterized a soil temperature (10 cm depth) response function:

$$F_{(T_{soil})} = a \, e^{(b \, T_{soil})}, \text{ and } Q_{10} = e^{10b}$$

(9)

Where, $F_{(T_{soil})}$ is the daily CH_4 flux parameterized by a first order exponential of soil temperature (T_{soil}, °C) with fitting coefficients a and b obtained from a least absolute residual optimization, and Q_{10} is the ratio of fluxes from a 10 °C temperature increase. The total uncertainty for approach A was assessed as the range in CH_4 budgets obtained across the $n = 50$ extrapolations above (each with its own soil temperature regression). We treat this simple variable estimate as the baseline gap-filling approach in this study.

2.5.2. Approach B: artificial neural networks (ANN)

Artificial neural networks (ANN) are increasingly used for gap-filling (CH_4) flux time series (e.g. Dengel et al., 2013; Knox et al., 2015; Sturtevant et al., 2016; Goodrich et al., 2016) due to (i) their capacity

for modeling data with varying temporal periodicity, and (ii) their freedom from any prior assumption regarding the functional relationship between independent and dependent variables (Papale et al. 2006; Moffat et al. 2007). Here, we followed established routines and employed a feedforward network with variable architecture complexity and tan-sigmoid transfer functions. Prior to network training, the 30-min flux time series was subsampled equally into training, validation and test subsets. The test subsets were withheld from initialization and validation of the individual network trainings and used only to infer uncertainty in the final chosen networks. Network training and validation were repeated numerous times with increasing complexity, i.e. by increasing the number of hidden layers and neurons per hidden layer.

The training variables tested included soil temperature (10 cm), air temperature, soil heat flux (average of 5 heat flux plates at 8 cm depth), photosynthetically active radiation (PAR), water table position, soil moisture, atmospheric pressure, and water vapor deficit. We first ranked these variables according to their correlation with the observed methane fluxes, and then added them step-wise into the training data set. After training and validation of each neural network, we computed the mean square error (MSE) and coefficient of determination of the modeled data compared to the withheld test data. Finally, we chose the network with the least number of training variables, lowest number of (hidden) layers and nodes, lowest MSE and highest R^2. The ANN routine including randomized subsampling, training and validation was repeated $n = 50$ times to calculate an ANN-derived ensemble distribution of gap-filled time series. The uncertainty of approach B was then assessed based on the ensemble range, with the ensemble mean used to gap-fill.

2.5.3. Approach C: Marginal distribution sampling (MDS) and mean diurnal course (MDC)

For approach C, missing 30-min fluxes were filled using averages from available observations under similar meteorological conditions on neighboring days (MDS) or based on the mean diurnal course aggregated from fluxes under similar conditions (MDC). The MDS approach employs a modified look up table accounting for auto-correlation of CH_4 flux time series. Similar conditions were defined as soil temperatures within 0.5 °C and air temperatures within 2.5 °C. The "neighboring days" criterion was iteratively increased from 1, 2, 7, 14, and 35 days, until data under similar conditions were available. The methodology is described in more detail in Reichstein et al. (2005) and Wutzler et al. (2018). We randomly introduced artificial gaps (25% of observations) and repeated the gap-filling procedure $n = 50$ times for both MDS and MDC approaches to infer the respective uncertainties based on the ensemble range.

2.6. Statistical analysis

Flux errors are typically not normally distributed (Hollinger and Richardson, 2005). Accordingly, Laplace (double exponential) distributions were used to describe the flux errors as $f(x \mid \mu, \beta) = \frac{1}{2\beta} e^{-|x-\mu|/\beta}$, where μ is the mean and β is a scaling factor related to the standard deviation ($\sigma = \sqrt{2}\beta$). Briefly, Laplace distributions are unimodal, but have a sharper peak (leptokurtic) than normal distributions. Geometric regression was employed when comparing two flux time series to account for uncertainty in both the regressor and dependent variable. Standard forecasting accuracy measures were used to evaluate performance of different gap-filling approaches on withheld observational data subsets, namely mean absolute error (MAE), root mean square error (RMSE), and bias error (BE; calculated as the mean of predicted minus observed values).

Uncertainties in the annual and campaign-long flux integrals were estimated assuming negligible autocorrelation in the random error ($\in$) and negligible systematic errors. Thus a standard error propagation

(Farrance and Frenkel, 2012) was performed as $\Delta F_{CH4} = \sqrt{\sum_i^o (\in_i)^2 + \sum_i^k (gapfill\ error_i)^2}$, where o and k refer to the number of observations and number of modeled fluxes within the integration interval, respectively. We neglected other (uncorrected for) systematic errors in this propagation as we expect them to be much smaller than the uncertainties discussed above. While assuming non-auto-correlated errors will in principle lead to a lower bound on the uncertainty, characterizing the auto-correlation of $\in$ is beyond the scope of this study.

3. Results and discussion

3.1. Flux attenuation

Analysis of cospectra revealed high frequency attenuation for both CH_4 systems (at $f \geq 0.08\,Hz$), whereas CO_2 cospectra followed expected behavior up to $> 0.2\,Hz$ indicating less high frequency loss. At the cospectral peak (frequencies of $\sim 0.16\,Hz$), cospectra for the LI-7700 fell below those for the TGA, while the reverse was true at higher frequencies, indicating different sources of high frequency attenuation between the CH_4 systems This finding agrees with theoretical expectations (e.g. tube attenuation only affected the TGA).

Methane cospectra also showed low frequency attenuation due to the applied de-trending algorithm, which appeared less pronounced for the TGA than for the LI-7700 relative to the idealized temperature spectrum. However, this apparent offset was proportional to the much larger covariance contribution from a trend in the raw TGA data as compared to the LI-7700 raw data (green and blue triangles, Fig. 1a).

Despite different frequency dependencies for spectral losses between the two CH_4 flux systems, estimates of total flux attenuation derived from empirical transfer functions were similar with median $\frac{\delta_c}{F_c} \pm$ standard deviations of 20 ± 5% (TGA), and 20 ± 5% (LI-7700). Of this 9 ± 4% were due to low frequency attenuation alone. Individual empirically determined transfer functions at times deviated from the idealized response ($0 \leq H(f) \leq 1$; see error bars in Fig. 1b) due to noise and incomplete trend removal (especially in the low frequencies for the TGA). Such behavior has also been observed at other sites (Aubinet et al., 1999; Peltola et al. 2013).

Estimates of flux attenuation derived from theoretical transfer functions were similar to the empirical values for the TGA (21 ± 7%), but systematically larger for the LI-7700 (25 ± 10%) (Fig. 2). Low frequency losses contributed 10 ± 8% to total flux attenuation. To elucidate the discrepancy in LI-7700 attenuation estimates we investigated individual theoretical transfer functions and found that observed and modeled attenuation disagreed mostly in the high frequency range (e.g. blue circles vs. dotted magenta line Fig. 1b), and further that the modeled losses due to sensor separation had the largest impact on overall attenuation. We hypothesize that violations of key assumptions within the analytical formulation of this transfer function (e.g. lack of differentiation between streamwise and cross-wind cospectra) contributed to the observed discrepancy (Horst and Lenschow, 2009). On an annual time scale, the cumulative mismatch of fluxes corrected with the empirical or the theoretical approach was $0.3\,gCH_4\,m^{-2}$ for the TGA, and $0.6\,gCH_4\,m^{-2}\,yr^{-1}$ for the LI-7700. This represented less than 4% of cumulative annual emissions. The small net impact on annual fluxes for the LI-7700 was due to the non-monotonic response of calculated fluxes (Eq. (3)) to increased CH_4 covariance (Fig. S6c).

To put the flux attenuation for the two CH_4 EC systems into context, we also calculated spectral losses for the LI-7500 CO_2/H_2O measurements. As suggested by the near-idealized cospectral shape (Fig. 1a) attenuation was small, with similar estimates derived from the theoretical and empirical approaches (median $\frac{\delta_c}{F_c} = 3 \pm 2\%$). Estimated (high frequency) spectral losses of our CH_4 covariance measurements are similar to previous reports. For example Peltola et al. (2014) reported a median attenuation range of ≈ 10–40% for 8 commercially available CH_4 gas analyzers deployed at about 6 m height (0.05–0.3 m horizontal separation) above an agriculturally managed peatland in the Netherlands. Iwata et al. (2014) reported 11% attenuation for the LI-7700 deployed at 3.35 m height (0.25 m horizontal separation) over a rice paddy in Japan, Goodrich et al. (2016) reported 15% median attenuation for the LI-7700 deployed 4.2 m (0.2 m horizontal separation) above a sedge tundra in Alaska, and Chu et al. (2014) reported LI-7700 flux attenuation to range from 20 to 30% at 2 m height above short canopy of a freshwater marsh at Lake Erie.

Overall, theoretical expectations of spectral losses did not always align with the observed cospectra. Thus we chose to apply the empirical approach for all subsequent analyses in this manuscript. After assessing the degree of systematic diurnal and seasonal variability in flux
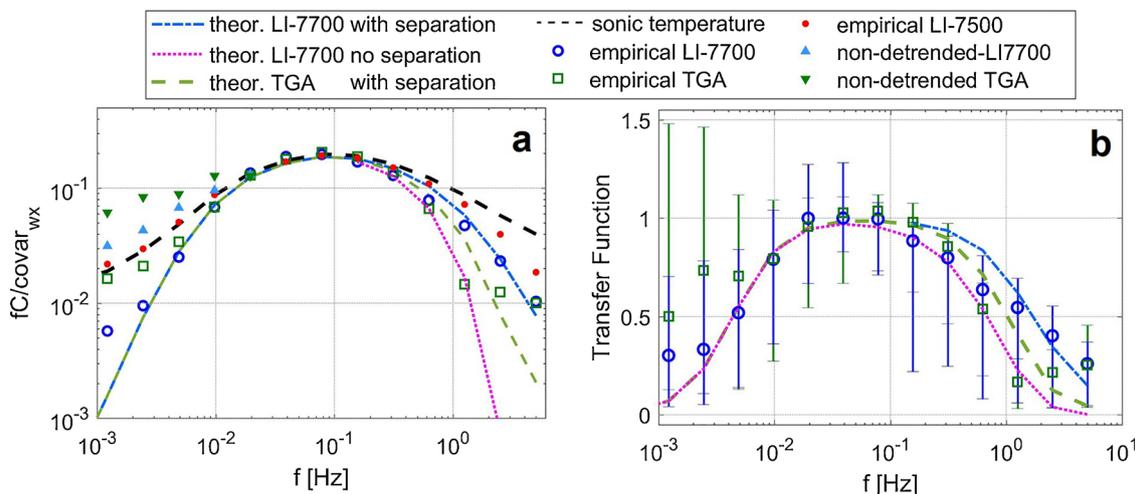
Fig. 1. Panel a shows absolute frequency weighted and normalized cospectra under unstable atmospheric conditions (L < 0) for sonic temperature (black dashed line), carbon dioxide (CO_2, red dots), and methane as measured by the closed path TGA (hollow green squares) and open path LI-7700 (hollow blue circles) analyzers as a function of frequency (f). Also shown are cospectra for non-detrended (i.e. raw) data from the TGA (solid green triangles) and the LI-7700 (solid blue triangles). Further, theoretical transfer functions were applied to the temperature cospectra to show the expected combined low- and high frequency attenuation for the TGA (green dashed line), the LI-7700 (magenta dotted line), and the LI-7700 assuming zero sensor separation (blue dash-dotted line). The plotted (co)spectra are an ensemble average of individual ($n = 800$) spectra screened for stationarity ratio < 0.3 and Obukhov-Length L < L n < 0. Panel b shows theoretical transfer functions and median empirical transfer functions (symbols) with inter-quantile-range (error bars) for the TGA (green, squares) and LI-7700 (blue, circles) analyzers. Broken lines denote theoretical transfer functions, similar to panel a.
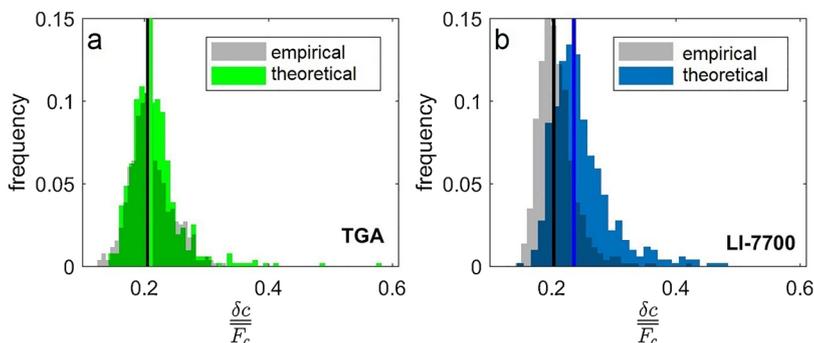
Fig. 2. Probability density distributions of relative flux attenuation (combined low- and high-pass filtering) for the closed path TGA (panel a), and open path LI-7700 (panel b) CH$_4$ analyzers. Results shown are based on theoretical (colored histograms) and empirical transfer functions (gray histograms) for quality-ensured 3-hr periods during stable and unstable conditions.

attenuation (Text S6) we chose to employ constant (year-round) spectral correction factors for each greenhouse gas flux system.

3.2. Flux precision & uncertainty

3.2.1. Noise & detection limits

In agreement with previous studies (Peltola et al., 2013, 2014; Rannik et al., 2016), instrumental noise contributions to flux uncertainty were negligible, accounting for only 3% ± 3% (median ± 1 σ) of the measured covariances for the TGA and 1% ± 2% for the LI-7700 (Fig. 3a). The typical absolute noise covariance was < 1 nmol m^{-2} s^{-1} for the interquartile range (IQR), which is on the lower end of values reported in a comprehensive inter-comparison study (Peltola et al., 2014), and similar to noise levels reported for eddy flux using cavity-ring-down spectrometers (G2311-f/G1301-f; Picarro Inc, Santa Clara, CA, USA). The TGA exhibited more noise than the LI-7700 during this study.

Flux detection limits were estimated following Wienhold et al. (1995), with median values of approximately 3 ± 2 (± 1σ) nmol m^{-2} s^{-1} for both sensors (Fig. 3b). For comparison, the 1st percentile of all measured fluxes was 2.0 nmol m^{-2} s^{-1} for the TGA and 2.8 nmol m^{-2} s^{-1} for the LI-7700. Both instruments thus yielded reliable CH$_4$ measurements for the flux magnitudes observed at this site. Peltola et al. (2014) reported similar CH$_4$ flux detection limits of 2–4 nmol m^{-2} s^{-1} in their assessment of 7 different gas analyzers.

#### 3.2.2. Turbulent CH4 sampling errors from the Finkelstein & Sim, 2001 (F& S) approach

The median fractional random errors for individual fluxes based on the F&S approach were 17% ± 10% (± 1σ) for the TGA and 14%

± 10% for the LI-7700 (Fig. 3c). These corresponded to absolute errors of 4 ± 3 nmol m^{-2} s^{-1} for the TGA and 3 ± 3 nmol m^{-2} s^{-1} for the LI-7700. These flux errors are comparable to those from a spring-summer field inter-comparison study (Peltola et al., 2013) over an oligotrophic fen in Finland with reported median errors ranging from 1.0 nmol m^{-2} s^{-1} to 5.6 nmol m^{-2} s^{-1}. Some site-to-site differences in absolute random flux errors are to be expected, as such errors scale with the measured flux (heteroscedasticity, Fig. S7). Fractional errors here were in good agreement with the Peltola et al. (2013) study, with distributions of $\frac{\sigma_F}{w'c'}$ generally peaking at less than 20% for both analyzers. The F&S random errors are per definition strictly positive, as they characterize the sampling error distribution, and in our study highly skewed (here, skewness > 1.7) towards large values, i.e. following a Burr type distribution.

Based on the statistical approaches presented here and above (**3.2.1**) both EC systems provided flux measurements with comparable precision, with the LI-7700 yielding slightly lower (by ≈1 nmol m^{-2} s^{-1} on average) random flux errors according to the F&S approach.

3.2.3. Differences between paired and repeated measurements

3.2.3.1. The paired differences (PD) approach.
Differences in observed fluxes followed a symmetrical distribution around a near-zero mean (Fig. 4), which, as in earlier studies (Hollinger and Richardson, 2005; Dragoni et al., 2007), followed a Laplace rather than a Gaussian distribution. Fitted distributions (Section 2.6, Fig. 4) were described by a median of 0.1 nmol m^{-2} s^{-1}, a standard deviation (σ) of 8.5 nmol m^{-2} s^{-1}, and an IQR of 8.2 nmol m^{-2} s^{-1}. The center 75% of observed differences were within μ ± 1σ. Skewness (0.32) was close to zero, indicating an almost symmetric shape. Thus the distribution of paired observations, reflecting the uncertainty due to the flux measurement
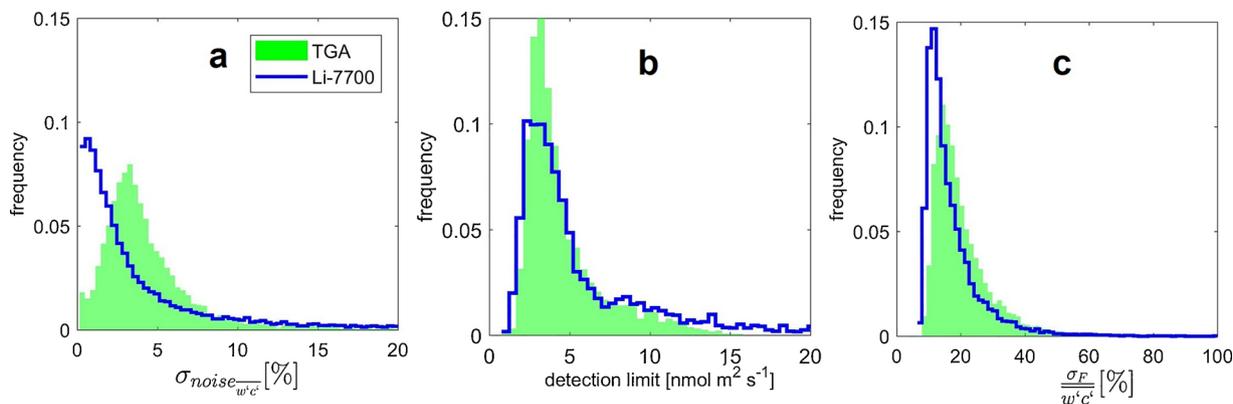
Fig. 3. frequency distributions of derived errors for the TGA system (green) and the LI-7700 system (blue). Panel a shows the relative error from instrumental noise, calculated as the second order auto-covariance (Eq. (8)). Panel b shows the fractional random flux error, estimated as the normalized standard deviation of the covariance (Eq. (7)). Panel c shows the absolute value of the CH$_4$ flux detection limit calculated as 1.96 times the standard deviation of the cross-covariance function (Wienhold et al. 1995; Rannik et al., 2016).
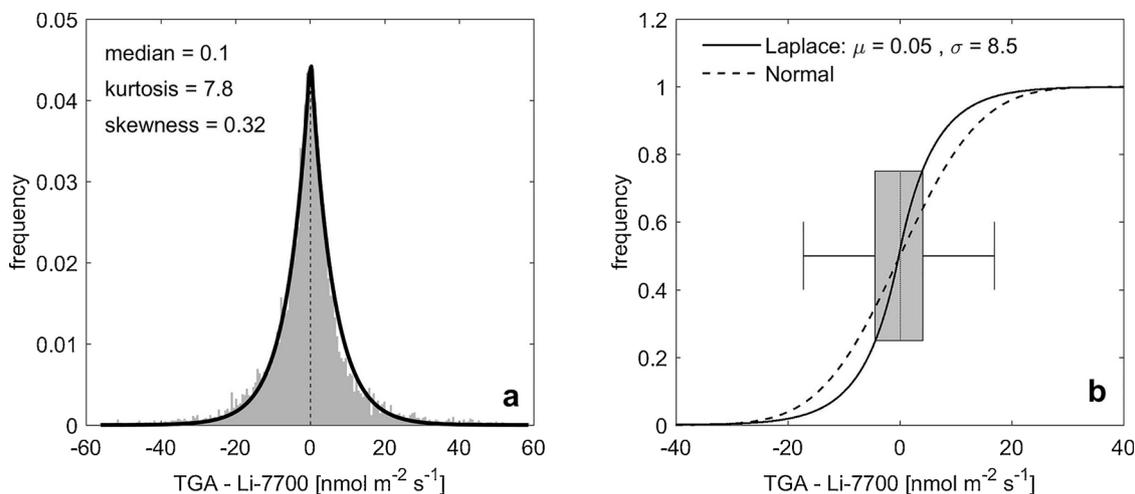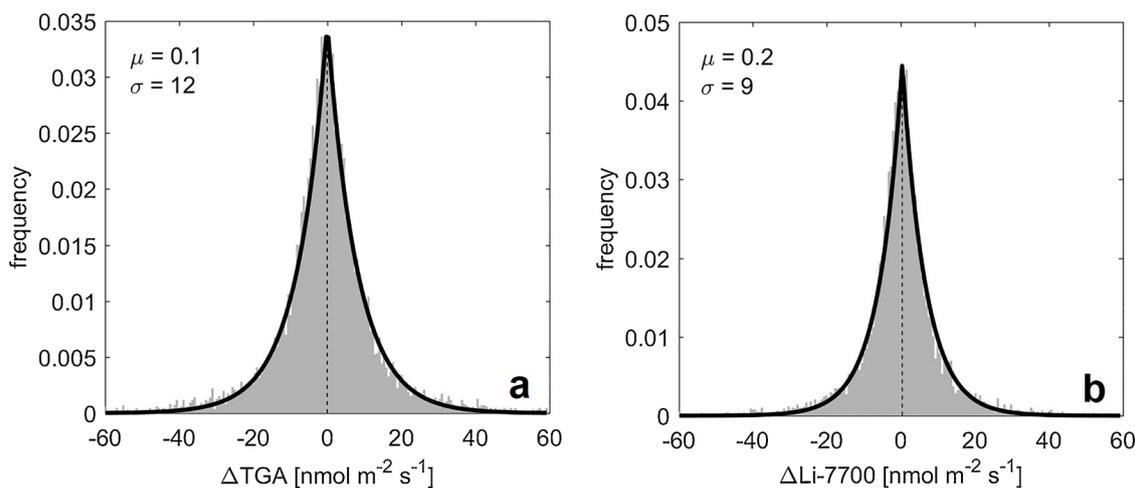
Fig. 4. Panel a shows the probability density distribution (gray histogram) of the 30-min CH_4 flux differences between the TGA and the LI-7700, with corresponding higher order statistics. Positive skewness denotes asymmetry towards larger TGA fluxes. A fitted Laplace distribution is overlaid (black line). Panel b shows the cumulative distributions for the Laplace distribution (black solid line) with fitting coefficients. For comparison, a normal distribution with the same mean (μ) and standard deviation (σ) is also plotted (dashed line). The overlaid box-whisker plot shows the IQR (gray box) and 1.5 times the IQR (error bars) for the measured differences.

systems, indicated negligible bias (0.1 nmol m^{-2} s^{-1}). This result is encouraging since LI-7700 flux measurements also incorporated uncertainty in the LE and H measurements (Eq. (3)). In the following we use two different approaches for estimating the overall random flux errors and assess the importance of the above derived uncertainties in that broader context.

3.2.3.2. The *Hollinger & Richardson, 2005* (H&R) approach.
Estimated errors from the H&R approach followed a double exponential distribution with near zero means (Fig. 5), and can thus directly be compared to the PD distribution. Inferred uncertainties were $\sigma = 9$ and 12 nmol m^{-2} s^{-1} for the LI-7700 and TGA, respectively, or 1.06× and 1.4× those from the PD approach. In other words, total flux uncertainty (as estimated by H&R) was larger than the uncertainty due to the CH_4 flux measurement systems (as estimated by PD). The H&R approach might be overestimating total flux errors due to potential contributions from non-stationarities (Hollinger & Richardson 2005). More importantly, however, the H&R approach (like F&S) accounts for

sampling errors due to turbulent stochasticity, which were shown previously to dominate uncertainty in turbulent transport (Rannik et al., 2016).

Another way to compare the 2 error estimates relying on paired measurements in time or on consecutive days (PD and H&R) is by quantifying the resulting relative errors. Fig. 6 thus plots the H&R and PD uncertainties normalized to the respective flux. We see that both relative errors exhibited a decreasing trend with increasing flux magnitude for $0 < F_{CH_4} < 150$ nmol m^{-2} s^{-1}. A similar trend was found for CO_2 flux errors with increasing CO_2 uptake (Hollinger & Richardson, 2005). The largest relative errors were found for near-zero fluxes, except in the case of the H&R estimates for the TGA which were largest for apparent CH_4 uptake. For fluxes > 150 nmol m^{-2} s^{-1} error estimates tend to increase and become noisy, which (similar to negative fluxes) was related to large variability within a small sample size in these bins. Here we found that the flux measurement system uncertainty was smaller than the random flux errors resulting from sampling errors and footprint heterogeneity. Specifically PD errors were 0.79× (TGA) and


Fig. 5. shows the probability density distributions (gray histograms) of flux errors derived from the H&R method. Also shown are fitted Laplace distributions (black lines) with mean (μ) and standard deviation (σ) for the TGA (panel a) and LI-7700 (panel b).
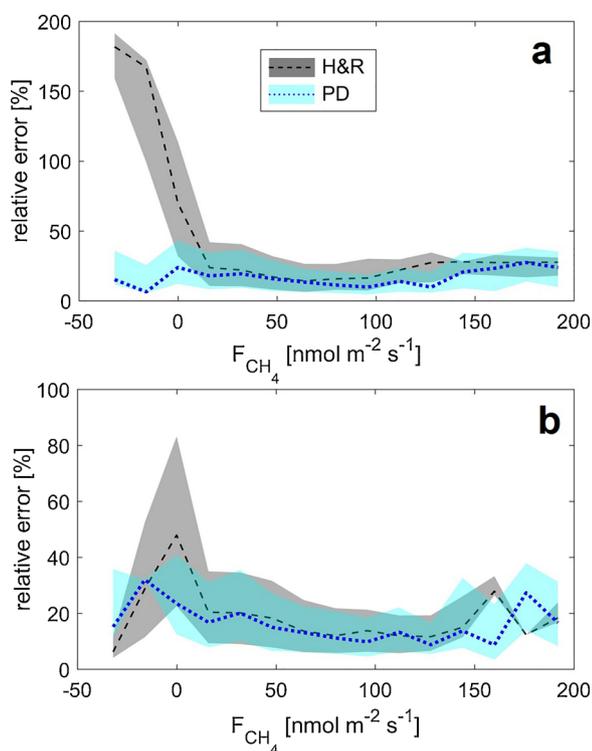
Fig. 6. The relationship between relative error estimates and CH_4 fluxes for the TGA (panel a) and the LI-7700 (panel b). Relative errors were estimated using the H&R approach (grey area with dashed line), the PD approach (blue area with dotted line). Lines denote medians, whereas areas denote the IQR of each bin.

$0.90\times$ (LI-7700) the H&R errors within the center 90 flux percentiles ($10 < F_{CH_4} < 90$ nmol m^{-2} s^{-1}). For these typical fluxes uncertainty estimates ranged from 6 to 41%, which is close to the 10 to 30% uncertainty range in turbulent fluxes reported by Rannik et al. (2016). If CH_4 flux uncertainties need to be predicted for future studies, random numbers can be drawn from the Laplace distribution parameters (Figs. 4 and 5).
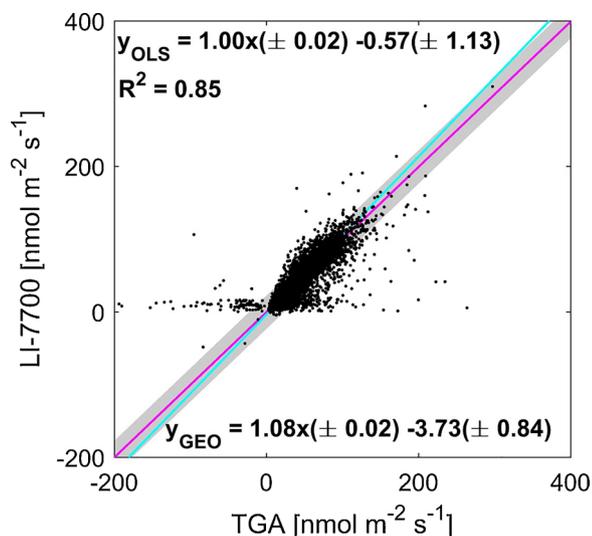
Fig. 7. scatter plot of 30-min CH_4 fluxes as measured by the TGA and LI-7700 systems. Overlaid are ordinary least squares (OLS) regression lines (magenta line with gray shaded 90% prediction bounds), and geometric (GEO) regression line (cyan).

3.3. Flux correlations

Regressed fluxes between the two sensors could adequately be described by a linear model (Fig. 7), with the largest residuals seen for negative TGA fluxes. Approximately 70% of the negative observations exceeded the corresponding flux detection limits but only 1% of these were observed from both systems. It is therefore questionable whether the measured negative net CH_4 fluxes were valid observations. While a soil CH_4 sink is expected under aerated conditions (Kirschke et al., 2013), the detected net CH_4 uptake did not correlate with low water table in this study. It is likely that these negative fluxes resulted from measurement errors (e.g. incomplete trend removal from the TGA measurements) that were not fully accounted for in quality control procedures.

While ordinary least squares regression of CH_4 fluxes measured with the LI-7700 against those measured with the TGA yielded a slope and intercept that were statistically not different from 1 and 0, respectively (Fig. 7), geometric regression yielded a greater-than-unity slope (1.08 ± 0.02, estimate $\pm$ 99% confidence interval) and a negative intercept (-3.0 ± 0.8). Correlation analysis thus indicated a tendency towards larger fluxes for the LI-7700 system, in contrast to the Laplace distribution parameters described above. In the following we investigate whether this small bias persists in gap-filled annual flux estimates derived using different gap-filling strategies

3.4. Assessing annual CH_4 budgets

For both the LI-7700 and TGA systems, only ~24% of the flux observations over the 3.5-year experiment passed all quality-control criteria. Hence, gap-filling strategies were needed to derive annual CH_4 budgets. In the following, three different gap-filling approaches and their associated uncertainties are presented.

3.4.1. Approach A: extrapolating 30-min fluxes to daily fluxes with subsequent gap-filling based on observed soil temperature response

For this approach, we hypothesized that 30-min fluxes could be reliably extrapolated to a daily value even if only a fraction of the 48 observations for the day was available. We found very little periodic variability in either of the CH_4 time series on an hourly timescale (Fig. 8a, b) for both absolute and normalized fluxes (Fig. 8c, d). Rather, most of the flux variability occurred on seasonal timescales. Similar analyses for sensible heat fluxes are shown for comparison in Fig. S8. We concluded that the CH_4 fluxes at this site undergo only marginal diurnal variations, which is consistent with prior findings at this site (Shurpali et al., 1993; Olson et al., 2013) and at other peatland sites where vegetation was not dominated by *Phragmites ssp.* (Jackowicz-Korczyński et al., 2010; Peltola et al. 2013; Rinne et al., 2007, 2018). Uncertainty analysis for the resulting extrapolations revealed little sensitivity to the minimum observation threshold (sec. 2.5.1) and to introduction of artificial gaps; resulting cumulative fluxes were consistent to within 7%.

To gap-fill those days with no valid 30-min flux measurements, we parameterized a response curve to soil temperatures; measurements from multiple depths were evaluated for inclusion. Regression analysis revealed the strongest correlation of fluxes with 10 cm soil temperatures, with consistent variance across the observed soil temperature range (Fig. 9). The relationship was fitted by a first-order exponential, yielding Q_{10} (relative increase over a temperature difference of 10 °C) = 2.9 (95% confidence interval: 1.9–4.3), RMSE = 9.5 nmol m^{-2} s^{-1}, and $R^2 = 0.88$. Our Q_{10} estimate is within the range for minerotrophic peat (1.5 to 6.4) reviewed in Segers (1998). It should be noted that EC derived Q_{10} values show large inter-site and inter-annual variability (e.g., 2.3–12; Jackowicz-Korczyński et al., 2010; Song et al., 2015; Peltola et al., 2013; Rinne et al., 2018). Rinne et al. (2018) argue that this spread in reported Q_{10} values might reflect non-temperature confounders and differing depths for soil temperature measurements.
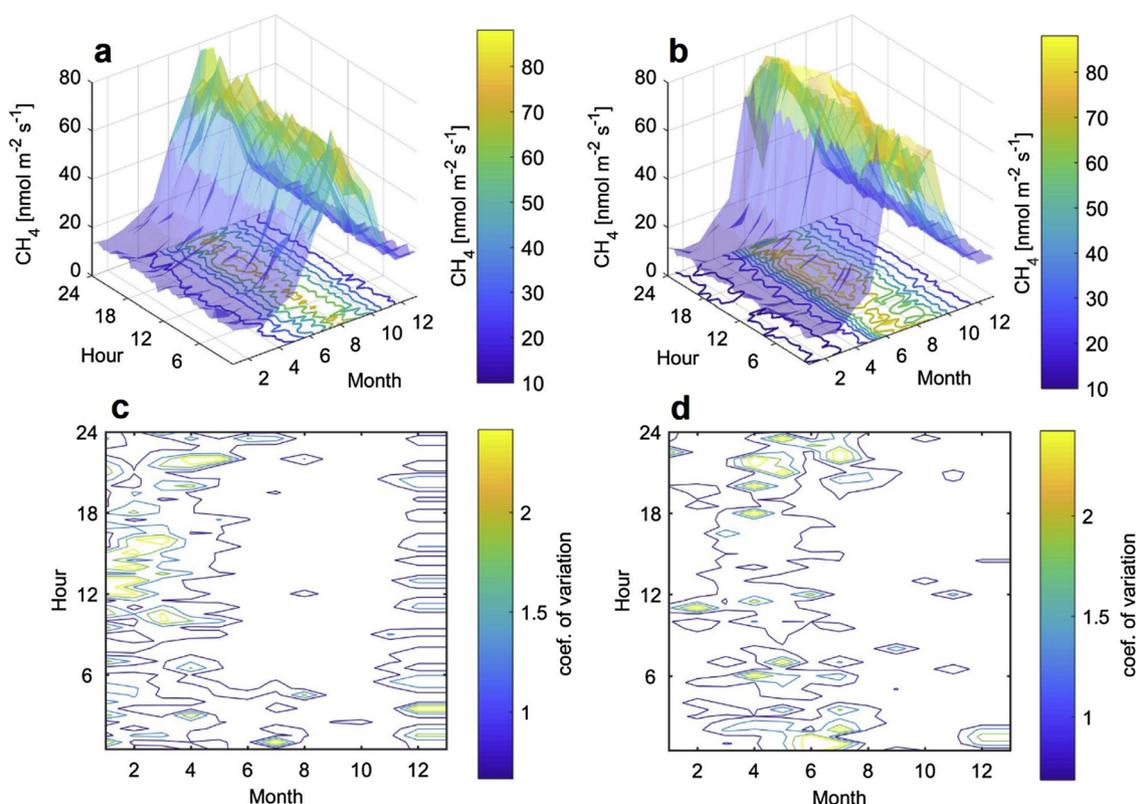
Fig. 8. Panel a and b summarize the temporal variance in CH_4 fluxes binned by half hour of the day (y-axis) and month of the year (x-axis). The color scale corresponds to the bin average CH_4 fluxes (z-axis and color scale) for the TGA (panel a) and the LI-7700 (panel b). Also shown are variations in fluxes normalized by the mean flux (coefficient of variation) for the TGA (panel c) and for the LI-7700 (panel d). Contours and surface colors are color coded by flux magnitude (panel a,b) and by the coefficient of variation (panel c,d).
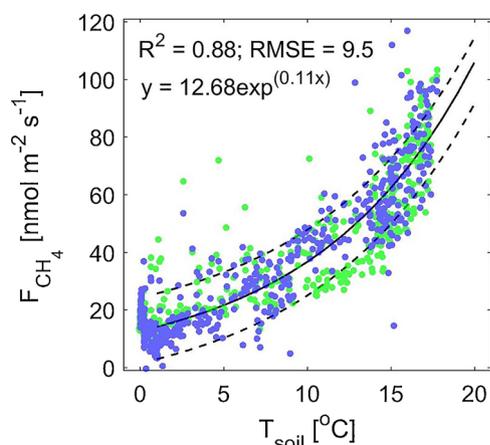
Fig. 9. scatter plot of daily CH_4 fluxes versus soil temperature (10 cm) for the TGA (green) and the LI-7700 (blue) datasets. Also shown is the best fit to a 1-term exponential $y = ae^{bx}$ (black solid line), with 90% prediction bounds (black dashed lines). Prediction bounds were [12.54, 12.81 nmol m^{-2} s^{-1}] for a, and [0.10, 0.11 °C] for b.

Here, flux regressions with water table position were much more complex than for soil temperature and did not follow a simple linear or log-linear relationship. Similar findings were reported from other peat moss vegetated wetlands (e.g. Rinne et al., 2007, 2018; Jackowicz-Korczyński et al., 2010).

Gap-filled daily fluxes from approach A showed good agreement between both EC systems (Fig. 10a, b). Over the course of 3.5 years, cumulative fluxes were 62.9 g − CH_4 m^{-2} (TGA) and 63.5 g − CH_4 m^{-2} (LI-7700) with gap-filling uncertainties of 0.9 g − CH_4 m^{-2} (TGA) and

1.1 g − CH_4 m^{-2} (LI-7700) (Table 2). At 30-min time scales, approach A yielded the worst performance of all gap-filling approaches tested here (Table 2). This was expected as this approach is designed for daily rather than half-hourly prediction. However, approach A was also subject to the largest positive bias errors resulting in the highest cumulative flux estimates. These biases were caused by inter-annual variability in soil temperature responses. Specifically 2015 was the least sensitive ($Q_{10} = 2.3$) as compared to the other 3 years ($Q_{10} \approx 3.1$), leading to over predicted fluxes in 2015. Thus the simple one-variable predictor model performed better for shorter (e.g. ≤ 1 year) time series. In the following we investigate how more complex gap-filling approaches with multiple predictors (ANN) and with moving time windows (MDS/MDC) perform as compared to the baseline approach.

3.4.2. Approach B: artificial neural networks (ANN)

Our second gap-filling strategy employed ANNs, which enabled direct gap-filling of the 30 min flux time series without prior extrapolation to daily values. Here, the final training data sets included as explanatory variables soil temperature, soil heat flux, water table position, and atmospheric pressure. ANN derived budgets yielded cumulative fluxes of 61.1 g − CH_4 m^{-2} when applied to the TGA time series, and 61.8 g − CH_4 m^{-2} when applied to the LI-7700. The coefficient of determination for the ANN predictions against withheld CH_4 flux data was $R^2 = 0.83$ (TGA) and $R^2 = 0.85$ (LI-7700) with improved forecasting performance and smaller bias compared to the baseline (approach A): MAE ≤ 8.9 nmol m^{-2} s^{-1} and RMSE ≤ 11.5 nmol m^{-2} s^{-1} (Table 2). We attribute this improvement in part to the fact that the ANN was able to resolve sub-daily variations of CH_4 emissions. ANN derived budgets were ∼3% smaller than with the baseline approach presented above (Tables 2 and 3).
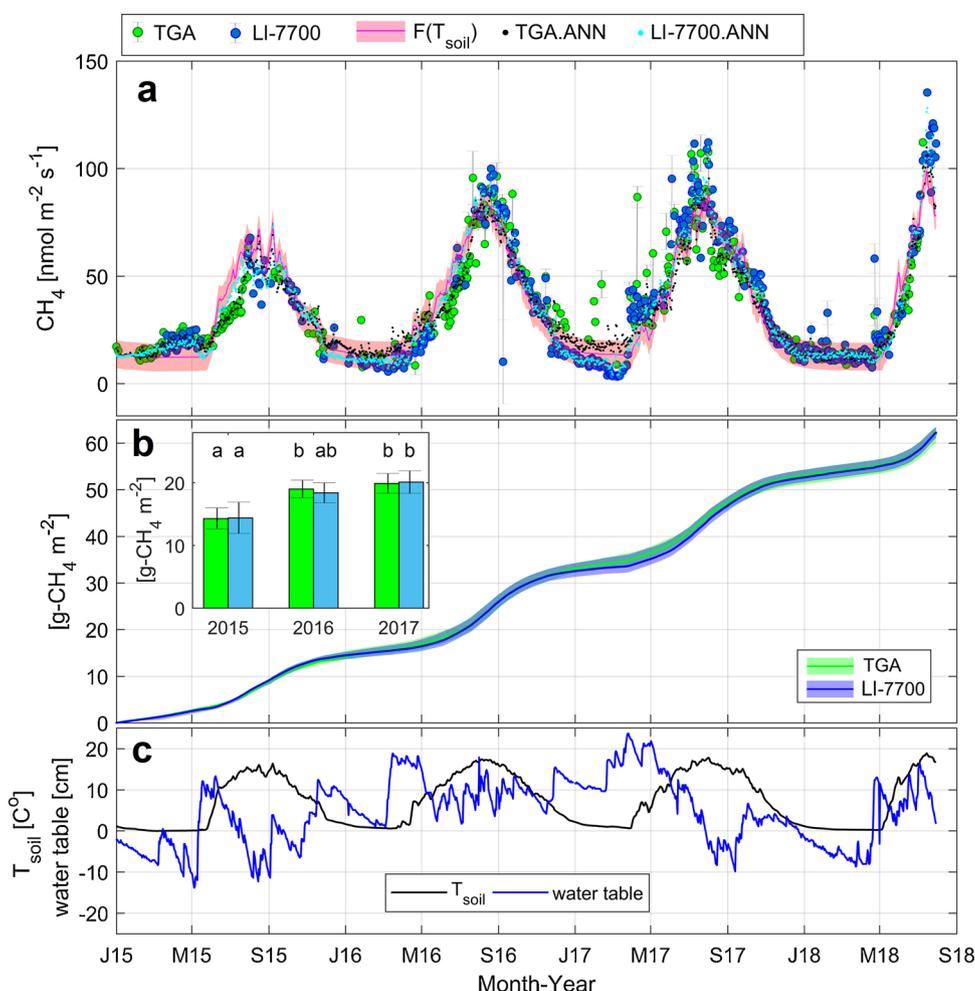
Fig. 10. Panel a shows an overview of 3.5 years of CH_4 flux measurements at Bog Lake Fen from 01/2015 (J15) to 08/2018 (S18). Measured and extrapolated daily fluxes for the TGA (green) and LI-7700 (blue) are shown together with associated extrapolation errors (error bars). Also shown are fluxes parameterized by soil temperature (red line) with associated uncertainty (red shaded area), and gap-filled fluxes based on ANN for the TGA (black dots) and the LI-7700 (cyan dots). Panel b shows cumulative fluxes for the TGA (green line) and LI-7700 (blue line). Shaded areas show the range of gap-filled budgets derived from all 4 gap-filling approaches evaluated here. The insert in panel b shows yearly CH_4 emissions (bar plots) and associated flux uncertainties (error bars). Superscript letters denote unique years with flux ± uncertainty different from other years: b > a, ab is not statistically distinguishable from either a or b. Panel c shows measured soil temperature (10 cm, black line) and water table position (blue line).

Table 2
Overview of gap-filled cumulative CH_4 flux budgets over 1307 days. Accuracy of filled data was evaluated on half-hourly observational data withheld from gap-filling (Section 2.5) and is presented as the mean absolute error (MAE), root mean square error (RMSE) and the bias error (BE). Gap-fill ranges represent the ensemble of budgets derived from bootstrapped datasets using the respective gap-filling method.

gap-fill method[*]	CH_4 analyzer	MAE [nmol m^{-2} s^{-1}]	RMSE [nmol m^{-2} s^{-1}]	BE [nmol m^{-2} s^{-1}]	R^2	cumulative flux [g-CH_4 m^{-2}]	gap-fill range [g-CH_4 m^{-2}]	relative gap-fill unc. [%]
Tsoil (A)	TGA	10.7	15.3	0.26	0.67	62.9	[62.5, 63.4]	1
ANN (B)	TGA	8.9	11.5	0.20	0.83	61.1	[60.0, 62.9]	5
MDS (C)	TGA	9.4	12.6	0.03	0.79	62.3	[61.4, 63.1]	3
MDC (C)	TGA	10	13.8	−0.10	0.76	62.4	[61.6, 63.1]	2
Tsoil (A)	LI-7700	9.9	12.4	0.23	0.75	63.5	[62.9, 64.0]	2
ANN (B)	LI-7700	7.4	8.4	−0.10	0.85	61.8	[61.0, 62.3]	2
MDS (C)	LI-7700	6.2	8.3	0.26	0.85	62.3	[61.8, 62.7]	1
MDC (C)	LI-7700	6.4	8.4	0.07	0.84	61.8	[61.2, 62.2]	2

* Fluxes were gap-filled using a soil temperature response model (Tsoil), artificial neural networks (ANN), marginal distribution sampling (MDS), and mean diurnal cycles (MDC). Details are provided in Section 2.5.

3.4.3. Approach C: Marginal distribution sampling (MDS) and mean diurnal course (MDC)

The MDS and the MDC approaches yielded cumulative fluxes of 62.3 g−CH_4 m^{-2}, and 62.4 g−CH_4 m^{-2}, respectively, when applied to the TGA time series, and 62.3 g−CH_4 m^{-2} and 61.8 g−CH_4 m^{-2} when applied to the LI-7700 time series. Thus, they fell in between the ANN budgets of 61.1–61.8 g-CH_4 m^{-2} and the T_{soil} derived budgets of 62.9–63.5 g-CH_4 m^{-2}. Accuracy and uncertainty were comparable between the MDS and MDC approaches, and overall performance was similar to that of ANN.

Over the 3.5 year period, the cumulative flux budgets derived across the four different gap-filling approaches and two different CH_4 flux

systems agreed remarkably well - to within 2.4 g−CH_4 m^{-2}, or 4% of the mean cumulative flux. Peltola et al. (2013) found similarly close agreement for a seasonal multi-sensor CH_4 study (4% over ≈180 days), and Goodrich et al. (2016) report 8% agreement between two CH_4 flux systems for a year-long campaign. In a 2 year study, Hommeltenberg et al. (2014) found ~10% sensitivity of annual CH_4 flux estimates to varying gap-filling approaches.

3.5. Annual flux uncertainty and interannual variability in CH_4 emissions

Hydro-meteorological conditions at the site varied strongly between the years 2015–2017. For instance, in 2015 the lowest peat

Table 3

Interannual variability in annual CH_4 emissions and associated uncertainty ranges.

year	CH_4 Analyzer	median[**]	gap-fill range[***]	gap-fill uncertainty	total uncertainty[*]		fraction gaps
		[g-CH_4 m^{-2} yr^{-1}]	[g-CH_4 m^{-2} yr^{-1}]	[%]	[g-CH_4 m^{-2} yr^{-1}]	[%]	[%]
2015	TGA	14.3 [a]	[13.7, 15.1]	9	1.7	12	78
	LI-7700	14.4 [a]	[13.8, 15.4]	11	2.5	17	85
2016	TGA	19 [b]	[18.7, 19.4]	4	1.4	7	80
	LI-7700	18.4 [ab]	[17.5, 19.0]	8	1.6	9	75
2017	TGA	19.9 [b]	[19.6, 20.7]	5	1.6	8	72
	LI-7700	20.1 [b]	[19.7, 20.8]	6	1.8	9	70

* Total uncertainties were estimated by standard error propagation of the gap-fill and the random flux errors (Section 2.6).

** Superscript letters denote unique years with flux ± uncertainty different from other years: b > a, ab is not statistically distinguishable from either a or b.

*** Combining all 4 gap-filling approaches.

temperatures and latest spring thaw onset were recorded (Fig. 11). Assessing the uncertainty in annual flux products arising from measurement and gap-filling errors is important, as these may exceed the inferred interannual variability. Our results show that cumulative emissions increased steadily from 2015 to 2017. In the case of the TGA time series, only 2015 showed a significant difference from the other 2 years (Table 3; Fig. 10b insert), whereas 2016 and 2017 were statistically indistinguishable. In case of the LI-7700, uncertainties were largest in 2015 (due to frequent gaps and hence high gap-filling errors), which as a result was only statistically distinguishable from 2017 (and not 2016). Based on the year-by-year analyses presented here (Table 3) we found the uncertainty of annual fluxes to range from 1.4 to $2.5\,g-CH_4\,m^{-2}\,yr^{-1}$ (7 to 17% of measured annual emissions).

Uncertainties in annual CH_4 wetland flux estimates have been reported previously and are summarized in Table 4. The literature shows that uncertainties in annual fluxes have been consistently estimated at < 33% with a median of 11%, with the exception of one boreal peatland site with near zero fluxes (Wang et al., 2017).

4. Recommendations and implications for CH_4 flux measurements and processing

Our results indicate that reliable CH_4 flux estimates can be achieved with close agreement between independent flux measurement systems. This suggests that a reliable global database of EC-derived CH_4 flux products can be obtained via systematic and standardized processing. To this end, we make the following recommendations and conclusions based on our data and analyses:
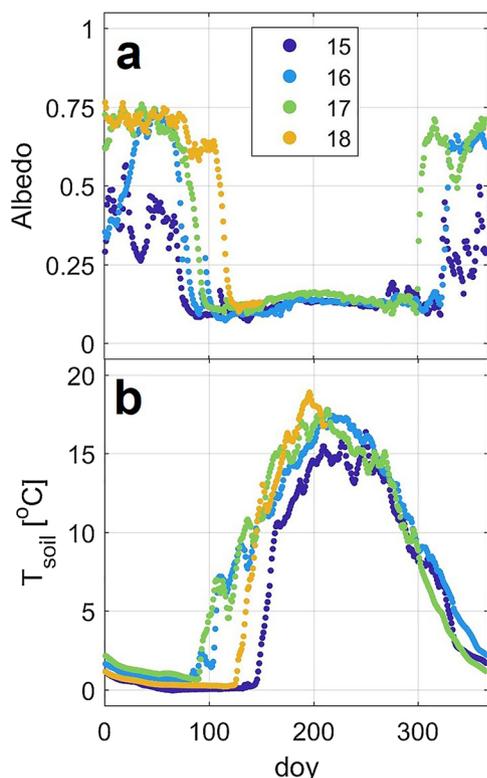
1 Flux underestimation associated with covariance attenuation for typical wetland CH_4 EC systems is on the order of 10 to 25%, and thus needs to be appropriately accounted for. We achieved consistent results between the empirical approach and theoretical approaches to within 4% of annual fluxes. For our data, the empirical approach (Aubinet et al., 1999; Foken et al., 2012), yielded the closest agreement between the EC systems evaluated here. After applying spectral corrections, remaining systematic error was estimated at < 2% of annual fluxes, and thus much smaller than random flux errors and gap-filling errors. Despite the substantial corrections required for the open-path LI-7700 measurements, the resulting final fluxes agreed well (on average ± 0.05 nmol m^{-2} s^{-1}) with those from the closed-path TGA system, demonstrating that the applied corrections are scientifically sound.

2 Based on statistical analysis of CH_4 time series, both the closed- and open-path systems provided a sufficient accuracy and precision to reliably characterize flux magnitudes and their predominant modes of variability at our study site. Estimated turbulent sampling errors were similar between both systems with a mode at ≈ 20% of measured covariances Median fluxes were ~1 order of magnitude above estimated flux detection limits 3 ± 2 (± 1σ) nmol m^{-2} s^{-1}. Thus, either open- or closed path EC systems can be suitably used depending on site characteristics and needs.

3 Random flux error estimates derived from differences between paired or repeated measurements in time suggested that the errors of the flux measurement system and flux calculation were smaller than errors due to the stochasticity of turbulent transport and that resulting from flux footprint heterogeneity. Thus it is feasible to merge CH_4 flux observations made with different measurement systems within global syntheses and interpret trends and variability among sites or years within the limitations of flux uncertainty derived from a single eddy covariance system. If CH_4 flux uncertainties

Fig. 11. Annual time series of daily soil temperature (panel a) and surface albedo (panel b), for 2015 (dark blue), 2016 (light blue), 2017 (green), and 2018 (orange).

Table 4

Literature review of annual wetland CH_4 flux estimates with associated relative uncertainties (ΔF_{CH4}).

wetland type	annual flux	ΔF_{CH4}	uncertainty includes		authors
	[g-CH_4 m^{-2} yr^{-1}]	[%]	gap-filling	random error	
boreal natural peatland	14.3–20.1[*]	7–17[*]	x	x	this study
boreal fen	12.6	8	x	x	Rinne et al. (2007)
managed fen on dairy farm	15.7–17[*]	17–33[*]	x	x	Kroon et al. (2010)
natural bog-pine	7.1	6	x	x	Hommeltenberg et al. (2014)
young wetland	70.7	1	x		Knox et al. (2015)
old wetland	51.6	3	x		Knox et al. (2015)
wet sedge tundra	6–6.5[*]	16–17[*]	x	x	Goodrich et al. (2016)
temperate mire	20–29[*]	5–14[*]	x		Fortuniak et al. (2017)
freshwater marsh	56.4–76[*]	9.1–11[*]	x	x	Chu et al. (2014)
aapa mire	5.5	14	x		Hargreaves et al. (2001)
arctic tundra	3.15	5	x		Wille et al. (2008)
boreal peatland	0.13–0.36	83–292[*]	x	x	Wang et al. (2017)
	median ΔF_{CH4}	11			

[*] Uncertainty for sites with multiple site years and flux systems are summarized as minimum – maximum value.

need to be predicted, fitted Laplace error distributions from this study can be used for random number generation.

4 We find that the CH_4 flux time series can be appropriately gap-filled using regression models, look-up tables, or machine learning approaches. The last two approaches performed the best in this study. Since established and publicly available tools exist for gap-filling flux products based on look up tables (Wutzler et al., 2018) we recommend this approach to facilitate transparency and reproducibility for synthesis purposes. However, for time series with long gaps (e.g. multiple months) machine learning approaches or simple regression models are advised. The performance of gap-filling techniques should be re-evaluated in future studies focusing on long term (e.g., decadal) flux time series.

5 We recommend estimating gap-filling uncertainty by generating an ensemble of bootstrapped time series with artificial data gaps. Despite the overall strong agreement between the gap-filled budgets obtained in this study, gap-filling uncertainties (up to 11% of the annual flux) were found to be on the same order of magnitude as the year-to-year emission differences.

6 The total uncertainty in annual CH_4 emissions is ≤17% for the dataset examined here. For a typical sub-boreal wetland flux of about 15 gC-CH_4 m^2, this yields an uncertainty range of ≈2.6 gC-CH_4 m^{-2}. Uncertainties need to be rigorously accounted for when assessing the carbon balance of peatland ecosystems, and when interpreting site-to-site or year-to-year variability in CH_4 emissions. Here, we observed that estimated annual emissions in 2017 were statistically distinguishable from the previous two years.

Appendix A. Supplementary data

Supplementary material related to this article can be found, in the online version, at doi:https://doi.org/10.1016/j.agrformet.2019.107638.

References

AmeriFlux, 2018. New Global CH4 Flux Initiative for Terrestrial Ecosystems. Online source: http://ameriflux.lbl.gov/new-global-ch4-flux-initiative-for-terrestrial-ecosystems/. Accessed on 2019/01/16. .

Aubinet, M., Grelle, A., Ibrom, A., Rannik, Ü., Moncrieff, J., Foken, T., Kowalski, A.S., Martin, P.H., Berbigier, P., Bernhofer, Ch, Clement, R., Elbers, J., Granier, A., Grünwald, T., Morgenstern, K., Pilegaard, K., Rebmann, C., Snijders, W., Valentini, R., Vesala, T., 1999. Estimates of the annual net carbon and Water Exchange of forests: the EUROFLUX methodology. In: Fitter, A.H., Raffaelli, D.G. (Eds.), Advances in Ecological Research. Academic Press, pp. 113–175. https://doi.org/10.1016/S0065-2504(08)60018-5.

Baldocchi, D., Falge, E., Gu, L., Olson, R., Hollinger, D., Running, S., Anthoni, P., Bernhofer, C., Davis, K., Evans, R., Fuentes, J., Goldstein, A., Katul, G., Law, B., Lee, X., Malhi, Y., Meyers, T., Munger, W., Oechel, W., Paw, U.K.T., Pilegaard, K., Schmid, H.P., Valentini, R., Verma, S., Vesala, T., Wilson, K., Wofsy, S., 2001. FLUXNET: a new tool to study the temporal and spatial variability of ecosystem-scale carbon dioxide, water vapor, and energy flux densities. Bull. Amer. Meteor. Soc. 82, 2415–2434. https://doi.org/10.1175/1520-0477(2001)082<2415:FANTTS>2.3.CO;2.

Baldocchi, D., Hincks, B.B., Meyers, T.P., 1988. Measuring biosphere-atmosphere exchanges of biologically related gases with micrometeorological methods. Ecology 69, 1331–1340. https://doi.org/10.2307/1941631.

Chu, H., Chen, J., Gottgens, J.F., Ouyang, Z., John, R., Czajkowski, K., Becker, R., 2014. Net ecosystem methane and carbon dioxide exchanges in a Lake Erie coastal marsh and a nearby cropland. J. Geophys. Res.: Biogeosci. 119, 722–740. https://doi.org/10.1002/2013JG002520.

Dengel, S., Zona, D., Sachs, T., Aurela, M., Jammet, M., Parmentier, F.J.W., Oechel, W., Vesala, T., 2013. Testing the applicability of neural networks as a gap-filling method using CH4 flux data from high latitude wetlands. Biogeosciences 10, 8185–8200. https://doi.org/10.5194/bg-10-8185-2013.

Detto, M., Verfaillie, J., Anderson, F., Xu, L., Baldocchi, D., 2011. Comparing laser-based open- and closed-path gas analyzers to measure methane fluxes using the eddy covariance method. Agric. For. Meteorol. 151, 1312–1324. https://doi.org/10.1016/j.agrformet.2011.05.014.

Dragoni, D., Schmid, H.P., Grimmond, C.S.B., Loescher, H.W., 2007. Uncertainty of annual net ecosystem productivity estimated using eddy covariance flux measurements. J. Geophys. Res. Atmos. 112. https://doi.org/10.1029/2006JD008149.

Farrance, I., Frenkel, R., 2012. Uncertainty of measurement: a review of the rules for calculating uncertainty components through functional relationships. Clin. Biochem. Rev. 33, 49–75.

Finkelstein, P.L., Sims, P.F., 2001. Sampling error in eddy correlation flux measurements. J. Geophys. Res. Atmos. 106, 3503–3509. https://doi.org/10.1029/2000JD900731.

Foken, T., Wichura, B., 1996. Tools for quality assessment of surface-based flux measurements. Agric. For. Meteorol. 78, 83–105. https://doi.org/10.1016/0168-1923(95)02248-1.

Foken, T., Aubinet, M., Leuning, R., 2012. The eddy covariance method. In: Aubinet, Marc, Vesala, T., Papale, D. (Eds.), Eddy Covariance. Springer, Dordrecht, Netherlands, pp. 1–19. https://doi.org/10.1007/978-94-007-2351-1_3.

Fortuniak, K., Pawlak, W., Bednorz, L., Grygoruk, M., Siedlecki, M., Zieliński, M., 2017. Methane and carbon dioxide fluxes of a temperate mire in Central Europe. Agric. For. Meteorol. 232, 306–318. https://doi.org/10.1016/j.agrformet.2016.08.023.

Fratini, G., Mauder, M., 2014. Towards a consistent eddy-covariance processing: an intercomparison of EddyPro and TK3. Atmos. Meas. Tech. 7, 2273–2281. https://doi.org/10.5194/amt-7-2273-2014.

Goodrich, J.P., Oechel, W.C., Gioli, B., Moreaux, V., Murphy, P.C., Burba, G., Zona, D., 2016. Impact of different eddy covariance sensors, site set-up, and maintenance on the annual balance of CO2 and CH4 in the harsh Arctic environment. Agric. For. Meteorol. 228–229, 239–251. https://doi.org/10.1016/j.agrformet.2016.07.008.

Hargreaves, K.J., Fowler, D., Pitcairn, C.E.R., Aurela, M., 2001. Annual methane emission

from Finnish mires estimated from eddy covariance campaign measurements. Theor. Appl. Climatol. 70, 203–213. https://doi.org/10.1007/s007040170015.

Hollinger, D.Y., Richardson, A.D., 2005. Uncertainty in eddy covariance measurements and its application to physiological models. Tree Physiol. 25, 873–885. https://doi.org/10.1093/treephys/25.7.873.

Hommeltenberg, J., Mauder, M., Drösler, M., Heidbach, K., Werle, P., Schmid, H.P., 2014. Ecosystem scale methane fluxes in a natural temperate bog-pine forest in southern Germany. Agric. For. Meteorol. 198–199, 273–284. https://doi.org/10.1016/j.agrformet.2014.08.017.

Horst, T.W., Lenschow, D.H., 2009. Attenuation of scalar fluxes measured with spatially-displaced sensors. Boundary-Layer Meteorol 130, 275–300. https://doi.org/10.1007/s10546-008-9348-0.

Iwata, H., Kosugi, Y., Ono, K., Mano, M., Sakabe, A., Miyata, A., Takahashi, K., 2014. Cross-validation of open-path and closed-path eddy-covariance techniques for observing methane fluxes. Boundary-Layer Meteorol 151, 95–118. https://doi.org/10.1007/s10546-013-9890-2.

Jackowicz-Korczyński, M., Christensen, T.R., Bäckstrand, K., Crill, P., Friborg, T., Mastepanov, M., Ström, L., 2010. Annual cycle of methane emission from a subarctic peatland. J. Geophys. Res. Biogeosci. 115. https://doi.org/10.1029/2008JG000913.

Kirschke, S., Bousquet, P., Ciais, P., Saunois, M., Canadell, J.G., Dlugokencky, E.J., Bergamaschi, P., Bergmann, D., Blake, D.R., Bruhwiler, L., Cameron-Smith, P., Castaldi, S., Chevallier, F., Feng, L., Fraser, A., Heimann, M., Hodson, E.L., Houweling, S., Josse, B., Fraser, P.J., Krummel, P.B., Lamarque, J.-F., Langenfelds, R.L., Quéré, C.L., Naik, V., O'Doherty, S., Palmer, P.I., Pison, I., Plummer, D., Poulter, B., Prinn, R.G., Rigby, M., Ringeval, B., Santini, M., Schmidt, M., Shindell, D.T., Simpson, I.J., Spahni, R., Steele, L.P., Strode, S.A., Sudo, K., Szopa, S., van der Werf, G.R., Voulgarakis, A., Weele, Mvan, Weiss, R.F., Williams, J.E., Zeng, G., 2013. Three decades of global methane sources and sinks. Nat. Geosci. 6, 813–823. https://doi.org/10.1038/ngeo1955.

Knox, S.H., Sturtevant, C., Matthes, J.H., Koteen, L., Verfaillie, J., Baldocchi, D., 2015. Agricultural peatland restoration: effects of land-use change on greenhouse gas (CO2 and CH4) fluxes in the Sacramento-San Joaquin Delta. Glob. Chang. Biol. 21, 750–765. https://doi.org/10.1111/gcb.12745.

Kottek, M., Grieser, J., Beck, C., Rudolf, B., Rubel, F., 2006. World Map of the Köppen-Geiger climate classification updated. Meteorol. Z. 259–263. https://doi.org/10.1127/0941-2948/2006/0130.

Kroon, P.S., Schrier-Uijl, A.P., Hensen, A., Veenendaal, E.M., Jonker, H.J.J., 2010. Annual balances of CH4 and N2O from a managed fen meadow using eddy covariance flux measurements. Eur. J. Soil Sci. 61, 773–784. https://doi.org/10.1111/j.1365-2389.2010.01273.x.

Lenschow, D.H., Wulfmeyer, V., Senff, C., 2000. Measuring second- through fourth-order moments in noisy data. J. Atmos. Oceanic Technol. 17, 1330–1347. https://doi.org/10.1175/1520-0426(2000)017<1330:MSTFOM>2.0.CO;2.

Mammarella, I., Peltola, O., Nordbo, A., Järvi, L., Rannik, Ü, 2016. Quantifying the uncertainty of eddy covariance fluxes due to the use of different software packages and combinations of processing steps in two contrasting ecosystems. Atmos. Meas. Tech. 9, 4915–4933. https://doi.org/10.5194/amt-9-4915-2016.

Massman, W.J., 2000. A simple method for estimating frequency response corrections for eddy covariance systems. Agric. For. Meteorol. 104, 185–198. https://doi.org/10.1016/S0168-1923(00)00164-7.

Massman, W.J., 2001. Reply to comment by Rannik on "A simple method for estimating frequency response corrections for eddy covariance systems.". Agric. For. Meteorol. 107, 247–251. https://doi.org/10.1016/S0168-1923(00)00237-9.

McDermitt, D., Burba, G., Xu, L., Anderson, T., Komissarov, A., Riensche, B., Schedlbauer, J., Starr, G., Zona, D., Oechel, W., Oberbauer, S., Hastings, S., 2011. A new low-power, open-path instrument for measuring methane flux by eddy covariance. Appl. Phys. B 102, 391–405. https://doi.org/10.1007/s00340-010-4307-0.

McMillen, R.T., 1988. An eddy correlation technique with extended applicability to non-simple terrain. Boundary-Layer Meteorol 43, 231–245. https://doi.org/10.1007/BF00128405.

Moffat, A.M., Papale, D., Reichstein, M., Hollinger, D.Y., Richardson, A.D., Barr, A.G., Beckstein, C., Braswell, B.H., Churkina, G., Desai, A.R., Falge, E., Gove, J.H., Heimann, M., Hui, D., Jarvis, A.J., Kattge, J., Noormets, A., Stauch, V.J., 2007. Comprehensive comparison of gap-filling techniques for eddy covariance net carbon fluxes. Agric. For. Meteorol. 147, 209–232. https://doi.org/10.1016/j.agrformet.2007.08.011.

Moore, C.J., 1986. Frequency response corrections for eddy correlation systems. Boundary-Layer Meteorol 37, 17–35. https://doi.org/10.1007/BF00122754.

Myhre, G., Shindell, D., Bréon, F.-M., Collins, W., Fuglestvedt, J., Huang, J., Koch, D., Lamarque, J.-F., Lee, D., Mendoza, B., Nakajima, T., Robock, A., Stephens, G., Takemura, T., Zhang, H., 2013. Anthropogenic and natural radiative forcing. In: Stocker, T.F., Qin, D., Plattner, G.-K., Tignor, M., Allen, S.K., Boschung, J., Nauels, A., Xia, Y., Bex, V., Midgley, P.M. (Eds.), Climate Change 2013: The Physical Science Basis. Contribution of Working Group I to the Fifth Assessment Report of the Intergovernmental Panel on Climate Change. Cambridge University Press, Cambridge, United Kingdom and New York, NY, USA.

Nemitz, E., Mammarella, I., Ibrom, A., Aurela, M., Burba, G.G., Dengel, S., Gielen, B., Grelle, A., Heinesch, B., Herbst, M., Hörtnagl, L., Klemedtsson, L., Lindroth, A., Lohila, A., McDermitt, D.K., Meier, P., Merbold, L., Nelson, D., Nicolini, G., Nilsson, M.B., Peltola, O., Rinne, J., Zahniser, M., 2018. Standardisation of eddy-covariance flux measurements of methane and nitrous oxide. Int. Agrophys. 32, 517–549. https://doi.org/10.1515/intag-2017-0042.

Nordbo, A., Katul, G., 2013. A wavelet-based correction method for eddy-covariance high-frequency losses in scalar concentration measurements. Boundary Layer Meteorol. 146, 81–102. https://doi.org/10.1007/s10546-012-9759-9.

Olson, D.M., Griffis, T.J., Noormets, A., Kolka, R., Chen, J., 2013. Interannual, seasonal,

and retrospective analysis of the methane and carbon dioxide budgets of a temperate peatland. J. Geophys. Res. Biogeosci. 118, 226–238. https://doi.org/10.1002/jgrg.20031.

Papale, D., Reichstein, M., Aubinet, M., Canfora, E., Bernhofer, C., Kutsch, W., Longdoz, B., Rambal, S., Valentini, R., Vesala, T., Yakir, D., 2006. Towards a standardized processing of Net Ecosystem Exchange measured with eddy covariance technique: algorithms and uncertainty estimation. Biogeosciences 3, 571–583. https://doi.org/10.5194/bg-3-571-2006.

Peltola, O., Mammarella, I., Haapanala, S., Burba, G., Vesala, T., 2013. Field inter-comparison of four methane gas analyzers suitable for eddy covariance flux measurements. Biogeosciences 10, 3749–3765. https://doi.org/10.5194/bg-10-3749-2013.

Peltola, O., Hensen, A., Helfter, C., Belelli Marchesini, L., Bosveld, F.C., van den Bulk, W.C.M., Elbers, J.A., Haapanala, S., Holst, J., Laurila, T., Lindroth, A., Nemitz, E., Röckmann, T., Vermeulen, A.T., Mammarella, I., 2014. Evaluating the performance of commonly used gas analysers for methane eddy covariance flux measurements: the InGOS inter-comparison field experiment. Biogeosciences 11, 3163–3186. https://doi.org/10.5194/bg-11-3163-2014.

Poulter, B., Bousquet, P., Canadell, J.G., Ciais, P., Peregon, A., Saunois, Marielle, Arora, V.K., Beerling, D.J., Brovkin, V., Jones, C.D., Joos, F., Gedney, Nicola, Ito, A., Kleinen, T., Koven, C.D., McDonald, K., Melton, J.R., Peng, C., Peng, Shushi, Prigent, C., Schroeder, R., Riley, W.J., Saito, M., Spahni, R., Tian, H., Taylor, Lyla, Viovy, N., Wilton, D., Wiltshire, A., Xu, X., Zhang, B., Zhang, Z., Zhu, Q., 2017. Global wetland contribution to 2000–2012 atmospheric methane growth rate dynamics. Environ. Res. Lett. 12, 094013. https://doi.org/10.1088/1748-9326/aa8391.

Rannik, Ü., Mammarella, I., Aalto, P., Keronen, P., Vesala, T., Kulmala, M., 2009. Long-term aerosol particle flux observations part I: uncertainties and time-average statistics. Atmos. Environ. 43, 3431–3439. https://doi.org/10.1016/j.atmosenv.2009.02.049.

Rannik, Ü., Peltola, O., Mammarella, I., 2016. Random uncertainties of flux measurements by the eddy covariance technique. Atmos. Meas. Tech. 9, 5163–5181. https://doi.org/10.5194/amt-9-5163-2016.

Rannik, Ü., Vesala, T., 1999. Autoregressive filtering versus linear detrending in estimation of fluxes by the eddy covariance method. Boundary. Meteorol. 91, 259–280. https://doi.org/10.1023/A:1001840416858.

Rebelo, L.-M., Finlayson, C.M., Nagabhatla, N., 2009. Remote sensing and GIS for wetland inventory, mapping and change analysis. J. Environ. Manage. 90, 2144–2153. https://doi.org/10.1016/j.jenvman.2007.06.027.

Reichstein, M., Falge, E., Baldocchi, D., Papale, D., Aubinet, M., Berbigier, P., Bernhofer, C., Buchmann, N., Gilmanov, T., Granier, A., Grünwald, T., Havránková, K., Ilvesniemi, H., Janous, D., Knohl, A., Laurila, T., Lohila, A., Loustau, D., Matteucci, G., Meyers, T., Miglietta, F., Ourcival, J.-M., Pumpanen, J., Rambal, S., Rotenberg, E., Sanz, M., Tenhunen, J., Seufert, G., Vaccari, F., Vesala, T., Yakir, D., Valentini, R., 2005. On the separation of net ecosystem exchange into assimilation and ecosystem respiration: review and improved algorithm. Glob. Chang. Biol. 11, 1424–1439. https://doi.org/10.1111/j.1365-2486.2005.001002.x.

Richardson, A.D., Aubinet, M., Barr, A.G., Hollinger, D.Y., Ibrom, A., Lasslop, G., Reichstein, M., 2012. Uncertainty quantification. In: Aubinet, M., Vesala, T., Papale, D. (Eds.), Eddy Covariance – A Practical Guide to Measurement and Data Analysis. Springer, Dodrecht, Heidelberg, London, New York, pp. 173–209. https://doi.org/10.1007/978-94-007-2351-1.

Rinne, J., Riutta, T., Pihlatie, M., Aurela, M., Haapanala, S., Tuovinen, J.P., Tuittila, E.St., Vesala, T., 2007. Annual cycle of methane emission from a boreal fen measured by the eddy covariance method. Tellus B 59, 449–457. https://doi.org/10.1111/j.1600-0889.2007.00261.x.

Rinne, J., Tuittila, E.-S., Peltola, O., Li, X., Raivonen, M., Alekseychik, P., Haapanala, S., Pihlatie, M., Aurela, M., Mammarella, I., Vesala, T., 2018. Temporal variation of ecosystem scale methane emission from a boreal fen in relation to temperature, water table position, and carbon dioxide fluxes. Global Biogeochem. Cycles 32, 1087–1106.

Saunois, M., Bousquet, P., Poulter, B., Peregon, A., Ciais, P., Canadell, J.G., Dlugokencky, E.J., Etiope, G., Bastviken, D., Houweling, S., Janssens-Maenhout, G., Tubiello, F.N., Castaldi, S., Jackson, R.B., Alexe, M., Arora, V.K., Beerling, D.J., Bergamaschi, P., Blake, D.R., Brailsford, G., Brovkin, V., Bruhwiler, L., Crevoisier, C., Crill, P., Covey, K., Curry, C., Frankenberg, C., Gedney, N., Höglund-Isaksson, L., Ishizawa, M., Ito, A., Joos, F., Kim, H.-S., Kleinen, T., Krummel, P., Lamarque, J.-F., Langenfelds, R., Locatelli, R., Machida, T., Maksyutov, S., McDonald, K.C., Marshall, J., Melton, J.R., Morino, I., Naik, V., O'Doherty, S., Parmentier, F.-J.W., Patra, P.K., Peng, C., Peng, S., Peters, G.P., Pison, I., Prigent, C., Prinn, R., Ramonet, M., Riley, W.J., Saito, M., Santini, M., Schroeder, R., Simpson, I.J., Spahni, R., Steele, P., Takizawa, A., Thornton, B.F., Tian, H., Tohjima, Y., Viovy, N., Voulgarakis, A., van Weele, M., van der Werf, G.R., Weiss, R., Wiedinmyer, C., Wilton, D.J., Wiltshire, A., Worthy, D., Wunch, D., Xu, X., Yoshida, Y., Zhang, B., Zhang, Z., Zhu, Q., 2016. The global methane budget 2000–2012. Earth Syst. Sci. Data 8, 697–751. https://doi.org/10.5194/essd-8-697-2016.

Schaefer, H., Fletcher, S.E.M., Veidt, C., Lassey, K.R., Brailsford, G.W., Bromley, T.M., Dlugokencky, E.J., Michel, S.E., Miller, J.B., Levin, I., Lowe, D.C., Martin, R.J., Vaughn, B.H., White, J.W.C., 2016. A 21st-century shift from fossil-fuel to biogenic methane emissions indicated by 13CH4. Science 352, 80–84. https://doi.org/10.1126/science.aad2705.

Segers, R., 1998. Methane production and methane consumption: a review of processes underlying wetland methane fluxes. Biogeochemistry 41, 23–51. https://doi.org/10.1023/A:1005929032764.

Shurpali, N.J., Verma, S.B., Clement, R.J., Billesbach, D.P., 1993. Seasonal distribution of methane flux in a Minnesota peatland measured by eddy correlation. J. Geophys. Res. Atmos. 98, 20649–20655. https://doi.org/10.1029/93JD02181.

Shurpali, N.J., Verma, S.B., Kim, J., Arkebauer, T.J., 1995. Carbon dioxide exchange in a

peatland ecosystem. J. Geophys. Res. 100, 14319. https://doi.org/10.1029/95JD01227.

Song, W., Wang, H., Wang, G., Chen, L., Jin, Z., Zhuang, Q., He, J.-S., 2015. Methane emissions from an alpine wetland on the Tibetan Plateau: neglected but vital contribution of the nongrowing season. J. Geophys. Res. Biogeosci. 120, 1475–1490. https://doi.org/10.1002/2015JG003043.

Sturtevant, C., Ruddell, B.L., Knox, S.H., Verfaillie, J., Matthes, J.H., Oikawa, P.Y., Baldocchi, D., 2016. Identifying scale-emergent, nonlinear, asynchronous processes of wetland methane exchange. J. Geophys. Res. Biogeosci. 121, 188–204. https://doi.org/10.1002/2015JG003054.

Tuzson, B., Hiller, R.V., Zeyer, K., Eugster, W., Neftel, A., Ammann, C., Emmenegger, L., 2010. Field intercomparison of two optical analyzers for CH4 eddy covariance flux measurements. Atmos. Meas. Tech. 3, 1519–1531. https://doi.org/10.5194/amt-3-1519-2010.

van den Berg, M., Ingwersen, J., Lamers, M., Streck, T., 2016. The role of *Phragmites* in the CH_4 and CO_2 fluxes in a minerotrophic peatland in southwest Germany. Biogeosciences 13, 6107–6119. https://doi.org/10.5194/bg-13-6107-2016.

Vickers, D., Mahrt, L., 1997. Quality control and flux sampling problems for tower and aircraft data. J. Atmos. Oceanic Technol. 14, 512–526. https://doi.org/10.1175/1520-0426(1997)014<0512:QCAFSP>2.0.CO;2.

Wang, M., Wu, J., Luan, J., Lafleur, P., Chen, H., Zhu, X., 2017. Near-zero methane emission from an abandoned boreal peatland pasture based on eddy covariance measurements. PLoS One 12, e0189692. https://doi.org/10.1371/journal.pone.0189692.

Webb, E.K., Pearman, G.I., Leuning, R., 1980. Correction of flux measurements for density effects due to heat and water vapour transfer. Q. J. R. Meteorol. Soc. 106, 85–100. https://doi.org/10.1002/qj.49710644707.

Wienhold, F.G., Welling, M., Harris, G.W., 1995. Micrometeorological measurement and source region analysis of nitrous oxide fluxes from an agricultural soil. Atmos. Environ. 29, 2219–2227. https://doi.org/10.1016/1352-2310(95)00165-U.

Wille, C., Kutzbach, L., Sachs, T., Wagner, D., Pfeiffer, E.-M., 2008. Methane emission from Siberian arctic polygonal tundra: eddy covariance measurements and modeling. Global Change Biol. 14, 1395–1408. https://doi.org/10.1111/j.1365-2486.2008.01586.x.

Wutzler, T., Lucas-Moffat, A., Migliavacca, M., Knauer, J., Sickel, K., Šigut, L., Menzer, O., Reichstein, M., 2018. Basic and extensible post-processing of eddy covariance flux data with REddyProc. Biogeosciences 15, 5015–5030. https://doi.org/10.5194/bg-15-5015-2018.